




Petrography and whole-rock geochemistry of Oligocene Barail Sandstones of Surma basin: Implications for tectono-provenance and paleoclimatic condition

PRADIP BORGHAIN¹, M FARUQUE HUSSAIN², DEVOJIT BEZBARUAH³,
V VANTHANGLIANA⁴, PARAKH PROTIM PHUKAN¹, MANASH PRATIM GOGOI¹
and BUBUL BHARALI^{4,*} 

¹Department of Petroleum Technology, Dibrugarh University, Dibrugarh, Assam 786 004, India.

²Department of Earth Science, Assam University, Silchar, Assam 788 011, India.

³Department of Applied Geology, Dibrugarh University, Dibrugarh, Assam 786 004, India.

⁴Department of Geology, Pachhunga University College, Aizawl, Mizoram 796 001, India.

*Corresponding author. e-mail: bubulearth@gmail.com

MS received 11 January 2020; revised 17 April 2020; accepted 29 April 2020

The Oligocene Barail Sandstones of Surma basin from parts of Champhai District of Mizoram, northeast India has been studied for their tectono-provenance setting using petrography and geochemistry. The studied sandstones are poor to moderately sorted, subarkosic to sub-litharenite and show dominance of quartz (avg. 54.46%) followed by feldspars (avg. 7.22%), rock fragments (avg. 4.98%), mica (avg. 5.89%), matrix (avg. 14.47%) and cement (avg. 12.98%). Dominance of polycrystalline and undulatory monocrystalline quartz indicates contribution from medium grade metamorphic sources, primarily of granite gneisses. High concentration of SiO₂ with moderate to low concentration of Al₂O₃, Fe₂O₃, MgO, Na₂O and K₂O resembles the composition of upper continental crust. Moreover, moderate to high concentration of Th and V, depleted value of Ni along with TiO₂/Zr suggests derivation of sediments from felsic sources. The ratios of Eu/Eu* (avg. 0.63) and La_N/Lu_N bears resemblance with the upper continental crust. Overall analyses show that the sediments were derived from the felsic terrain of neighbouring orogens probably represented by granite-gneisses and have undergone a moderate degree of weathering (avg. values of CIA: 70.20, CIW: 81.03, PIA: 77.63, WIP: 38.45, ICV: 1.06, I_w = 2) in a semi-humid to humid climatic conditions [$Q_p/(F + RF):Q_t/(F + RF) = 0.20$].

Keywords. Petrography; geochemistry; Barail Sandstone; Surma basin; Mizoram.

1. Introduction

Mizoram Fold Belt (MFB) is the easternmost extension of Surma basin, covering an area of about 25,000 km², accommodates about 5000 m thick sequence of Tertiary sediments. The entire terrain is hilly and bounded in the west by Tripura and the Chittagong Hill tracts (Bangladesh),

in the north by Assam and Manipur, in the east by Chin Hills and in the south by Arakan Hill tracts (Myanmar). Location of the various geotectonic domains associated with the MFB is represented in figure 1(A) (Hussain and Bharali 2019). The Tertiary sequences of MFB have been divided into Barail Group (Late Oligocene), Surma Group (Upper Oligocene–Miocene) and the

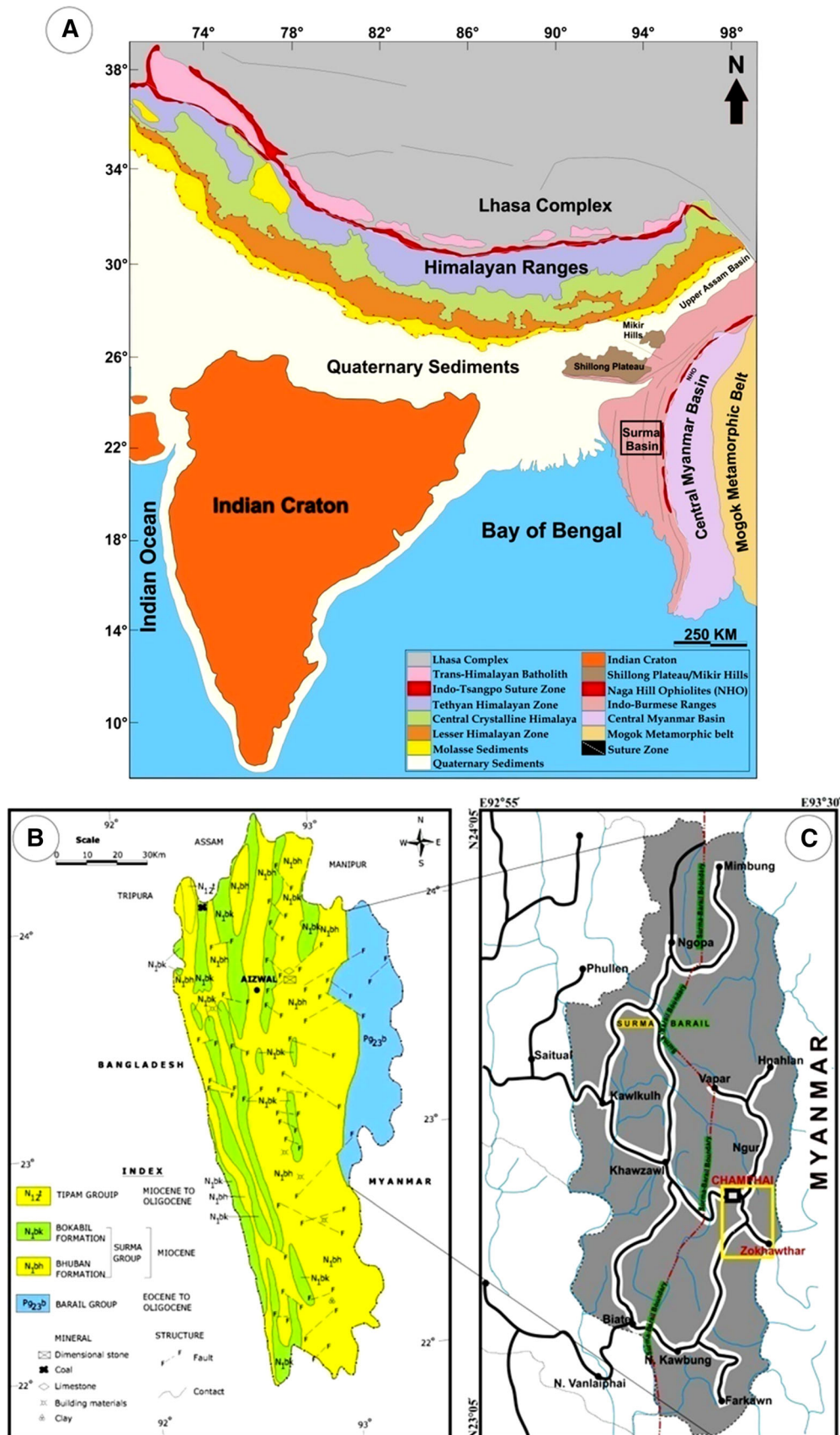


Figure 1. (A) Geological map of India with the subcontinents showing the various geo-tectonic domains associated with the Surma Basin (Hussain and Bharali 2019), (B) geological map of Mizoram (Bhaduri 2011), and (C) map showing the study area (yellow box).

Tipam Group (Late Miocene–Early Pliocene). The stratigraphic succession of MFB is presented in table 1. The evolution of Surma basin started with the deposition of Barail sediments which forms the base for the deposition of Miocene Surma Group of rocks. Barail sediments, however, are thrust over the Surma Group of rocks along Indo-Burma International Border (Dasgupta 1984) (figure 1B). MFB is composed of series of longitudinal folds arranged en-echelon. The anticlines are long and narrow, while the associated synclines are broad with well developed valleys (Ram and Venkataraman 1984). Owing to the inaccessibility of the terrain, the geological investigation in Mizoram is meager. The early work were done by La Touche (1891), Hayman (1937) and Franklin (1948). Nevertheless Ganju (1975), Nandy *et al.* (1983), Dasgupta (1984) and Tiwari *et al.* (2003, 2007, 2011) provided valuable information on the regional geological framework including tectonics, paleontology, and magneto-

stratigraphy, etc., of the basin. Geochemical studies on these rocks has not been taken up on a large scale except for the two recent publications of Sawant *et al.* (2017) and Hussain and Bharali (2019).

Present investigation concerns the study of provenance, tectonic setting and paleoclimate conditions prevailing during the deposition of the Barail sediments in eastern part of MFB based on petrography and whole-rock geochemistry. The petrography and geochemistry of clastic sedimentary rocks provide valuable information for understanding the tectonic setting, provenance, paleoweathering, paleoclimate and furthermore paleogeographic reconstruction of sedimentary basin (Basu *et al.* 1975; Dickinson and Suczek 1979; Dickinson 1983; Bhatia 1983; Suttner and Dutta 1986; McLennan *et al.* 1993; Cullers 2000; Gu *et al.* 2002; Paikaray *et al.* 2008; Armstrong-Altrin 2009; Saha *et al.* 2010, 2017; Chaudhuri *et al.* 2018, 2019, 2020).

Table 1. Geological succession of Mizoram Fold Belt (Ganju 1975).

Age	Group	Formation	Unit	Generalized lithology	
Recent	Alluvium			Silt, clay and gravel	
-----Unconformity-----					
Early Pliocene to Late Miocene	Tipam (+900 m)			Friable sandstone with occasional clay bands	
-----Conformable and transitional contact-----					
Miocene to Upper Oligocene	S u r m a (+5950 m)	Bokabil (+950 m)		Shale, siltstone and sandstone	
		-----Conformable and transitional contact-----			
		Bhuban (5000 m)	Upper Bhuban (1100 m)	Arenaceous predominating with sandstone, shale and siltstone	
			-----Conformable and transitional contact--		
			Middle Bhuban (3000 m)	Argillaceous predominating with shale, siltstone-shale alternations and sandstone	
-----Conformable and transitional contact--					
		Lower Bhuban (900 m)	Arenaceous predominating with sandstone and silty-shale		
-----Unconformity obliterated by faults-----					
Oligocene	Barail (+3000 m)			Shale, siltstone and sandstone	
-----Lower contact not seen-----					

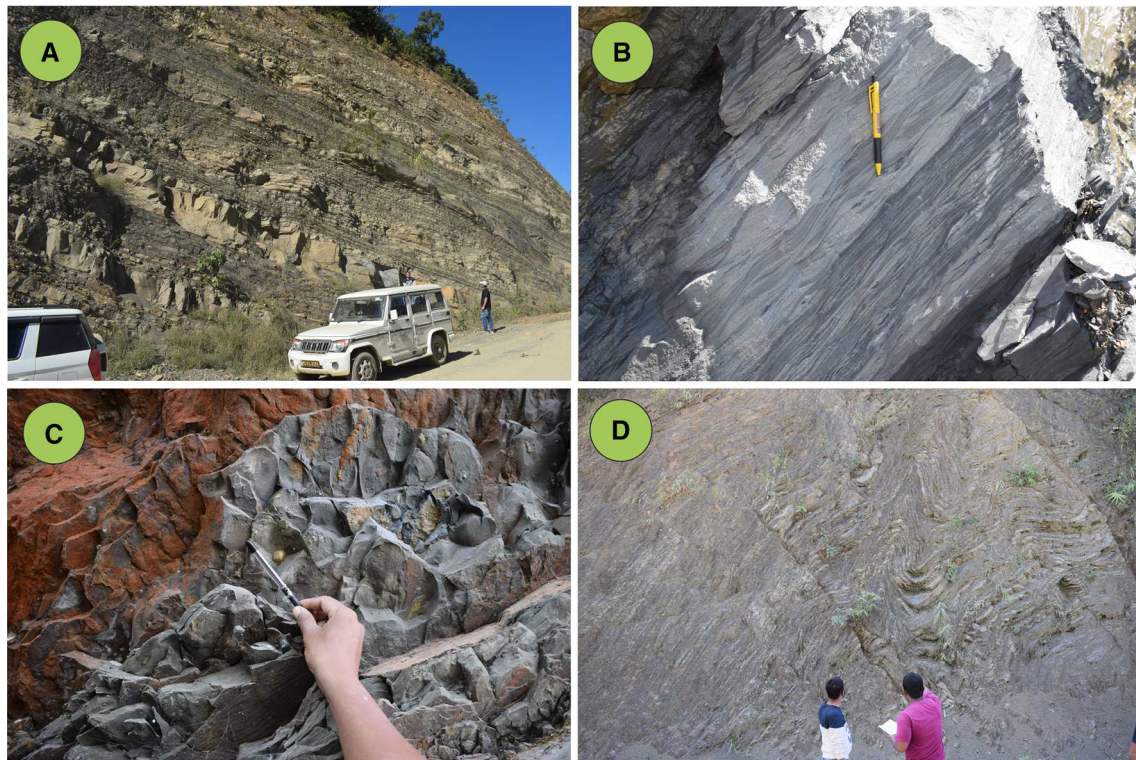


Figure 2. Field photographs of the study area. (A) Thick bedded sandstones alternate with shale and siltstones; (B) flaser and lenticular bedding developed in Barail Sandstones; (C) ripple marks, and (D) multiple phases of folding developed within alternate bands of shale, siltstone and sandstone.

2. Geology of the study area

The present study has been conducted between Champhai and Zokhawthar located at the eastern margin of Mizoram. Field traverse is about 25 km that covers within the latitude $N23^{\circ}28.435'$ – $N23^{\circ}21.792'$ and the longitude $E93^{\circ}20.007'$ – $E93^{\circ}23.284'$ with an average elevation of 1,300 m (MSL) (figure 1). The litho-association of the study area comprises of sandstones, shale and siltstones stacked in layers of alternate bands (figure 2A). Sandstones are generally buff coloured, fine to medium grained and show massive bedded character at certain places, while shales are dark grey coloured, hard and compact. The litho-association remarks a general coarsening upward sequence, the base of which is characterized by shale, gradually changing to siltstone and finally to sandstone (figure 2A). Sedimentary structures like lenticular and flaser bedding (figure 2B) and ripple marks (figure 2C) are observed in the field. Presence of a number of faults, folds and shear zones disturb the entire sequence (figure 2D). A representation of the outcropped litho-column of the studied section is shown in figure 3.

3. Methodology

Sixteen representative Barail sandstone samples were collected by using Portable Hand Drill Machine from the outcrops in the study area (figure 3). Petrographic study was carried out on rock thin sections prepared from air dried, araldite-impregnated sample using Buehler vacuum impregnation equipment. A Leica-DM750P Trinocular Polarizing Microscope fitted with CCD camera and Leica Image Analyser (LAV) is used for the petrographic study. The modal analysis was done by counting 500 points per thin section following the Gazzi–Dickinson (1966) method and the results are shown in table 2.

The geochemical analysis for 20 representative samples was carried out at National Geophysical Research Institute (NGRI), Hyderabad, India. The major oxides were analysed with Axism AX 4 kW Sequential Wavelength Dispersive-X Ray Fluorescence Spectrometer (WD-XRF). Trace and rare earth element analysis were carried out with High Resolution-Inductively Coupled Plasma Mass Spectrometer (HR-ICP-MS). Powdered samples (200 mesh size) were used to prepare pressed pellet for the determination of major oxides by using the

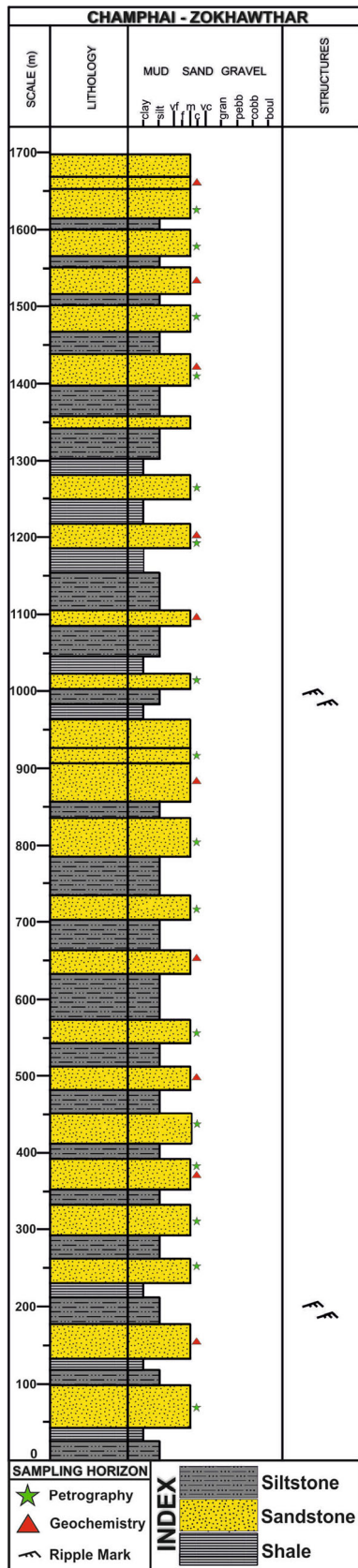


Figure 3. Lithocolumn of Champhai–Zokhawthar road section showing the various litho-association including the sampling horizon.

WD-X-Ray Fluorescence Spectrometer. For trace and rare earth element analysis, the powdered samples were dissolved in HF:HNO₃ solution using an open acid digestion technique. The sample solutions were analysed by using HR-ICP-MS. GSR 4 was used as a standard for calculating trace and rare earth elements. The results of geochemical analysis are shown in table 3.

4. Results

4.1 Sandstone petrography

Quartz, the predominant detrital framework grain in all the studied samples, occurs as monocrySTALLINE undulatory (avg. 24.98%), monocrySTALLINE non-undulatory (avg. 18.70%), and polycrySTALLINE varieties of 2–3 units (avg. 3.49%) and >3 units (avg. 7.29%). Both varieties of monocrySTALLINE quartz occur as subangular to subrounded grains (figure 4A), whereas polycrySTALLINE quartz varieties exhibit elongate, concavo-convex and sutured contacts (figure 4B). Few monocrySTALLINE quartz shows inclusion of zircon (figure 4B). Feldspars (avg. 7.22%) are mostly subangular to subrounded and occur as plagioclase (figure 4C) and K-feldspar in the studied samples. Mica (avg. 5.89%) occurs both as muscovite and biotite in the Barail Sandstone. They occur as lath-shape or tiny to large elongate flakes with frayed ends and muscovite dominates over biotite. Some of the mica flakes show compactional effects, as they exhibit jagged corners with micro fractures and kink bend (figure 4D) around detrital grains. Rock fragments of both sedimentary and metamorphic rocks are present in the studied sandstone and constitute an average 4.98% of the total rock volume. Rock fragments with gneissic and schistose fabric (figure 4E) constitute the metamorphic rock fragments, whereas shale and chert (figure 4F) constitute the sedimentary rock fragments. Amongst all the different varieties of rock fragments, the metamorphic types are dominating over the others with minor amount of volcanic rock fragments (figure 5A). Some of the weaker sedimentary rock fragments and the low grade metamorphic lithic fragments are converted to pseudomatrix (figure 5B and C) under compaction effects. Matrix (avg. 14.47%) is present as a complex mixture of finely constituted recrystallized material (<4 μm) filling the intergranular pore spaces. Three types of cements are found in Barail Sandstones. The silica

Table 2. Modal count of petrographic study of thin sections.

Sample no.	Quartz			Feldspar			Rock fragments			Cement			Recalculated %					
	Q _{Mu}	Q _{Mnu}	Q _{P-2-3}	Q _{P>3}	P _{Ca/Na}	F _K	RF _{Ig.}	RF _{Sed.}	RF _{Met.}	C _{Sil}	C _{Clay}	C _{Fer}	C _{Cal}	Matrix	Chert	Q	F	L
CT8	19.97	14.21	5.58	10.49	7.11	1.86	0.00	1.02	4.06	3.05	8.80	0.00	0.00	13.87	3.89	78.16	13.95	7.89
CZ4	29.94	13.63	2.50	8.06	3.45	0.00	0.00	1.34	2.69	4.03	4.03	0.00	0.00	15.93	5.37	87.85	5.61	6.54
CZ3	28.96	21.04	1.98	6.65	3.96	0.00	0.00	1.26	7.01	5.04	6.12	0.00	0.00	17.45	0.00	82.74	5.58	11.68
CT24	19.47	23.43	1.98	5.45	8.58	1.82	0.00	0.00	6.27	1.98	0.00	0.00	14.52	9.41	1.82	75.12	15.52	9.36
CZ14	28.65	13.85	8.92	8.92	4.17	2.09	0.00	1.71	5.12	2.09	3.98	0.00	0.00	15.75	0.00	82.17	8.53	9.30
CT23	25.42	17.28	4.65	7.14	6.31	1.99	0.00	0.00	4.49	2.16	3.65	1.00	0.00	17.11	0.00	80.99	12.35	6.67
CT7	18.77	24.40	4.44	7.17	8.02	1.19	0.00	0.00	5.46	1.19	4.44	0.68	0.00	14.16	2.05	78.87	13.27	7.86
CT31	19.93	24.95	1.86	5.59	8.38	1.86	0.00	0.00	5.96	2.23	0.00	0.00	13.04	9.12	1.86	76.36	14.95	8.70
CZ35	21.89	9.70	6.95	9.83	5.50	0.00	0.00	0.00	7.60	1.18	4.33	0.00	12.84	8.26	7.47	78.68	8.96	12.37
CZ32	27.37	19.93	1.49	6.33	5.03	0.74	0.00	0.00	8.01	3.17	2.42	0.00	0.00	14.53	4.10	80.00	8.38	11.62
CZ29	31.93	16.63	2.68	8.60	6.69	1.34	0.00	0.00	5.35	3.06	4.97	0.00	0.00	10.13	2.87	81.72	10.97	7.31
CZ36	30.92	19.96	1.37	5.48	6.26	2.74	0.00	0.00	4.89	3.52	7.24	0.00	0.00	12.33	0.00	80.60	12.57	6.83
CZ37	23.80	20.46	1.67	6.89	4.80	1.25	0.00	0.00	0.00	4.59	7.10	0.00	0.00	20.46	2.30	89.72	10.28	0.00
CZ38	26.14	19.71	2.49	6.02	5.39	1.04	0.00	0.00	2.90	3.11	5.81	0.00	0.00	18.26	3.32	85.34	10.10	4.56
CZ42	26.41	19.81	3.69	6.99	4.85	1.94	0.00	0.00	0.00	2.72	6.60	0.00	0.00	18.45	2.72	89.33	10.67	0.00
CZ43	26.10	20.22	3.68	7.17	5.51	1.65	0.00	0.00	4.60	2.21	4.78	0.00	0.00	16.36	1.84	82.93	10.40	6.67

Note. Q_{Mu}: monocrytalline undulatory quartz, Q_{Mnu}: monocrytalline non-undulatory quartz, Q_{P-2-3}: polycrytalline quartz with 2-3 grains per quartz, Q_{P>3}: polycrytalline quartz with >3 grains per quartz, P_{Ca/Na}: plagioclase, F_K: potash feldspar, RF_{Ig.}: igneous rock fragment, RF_{Sed.}: sedimentary rock fragment, RF_{Met.}: metamorphic rock fragment, C_{Sil}: siliceous cement, C_{Clay}: clay cement, C_{Fer}: ferruginous cement, C_{Cal}: carbonaceous/calcite cement.

Table 3. Table showing major elements (wt. %), trace elements (ppm), rare earth elements (ppm), and their corresponding elemental ratios with various weathering indices.

Oxides/elements	BS-16	BS-21	BS-25	BS-29	BS-36	BS-38	BS-46	BS-53	BS-54	BS-56	UCC	GLOSS	PAAS	NASC
SiO ₂	73.65	75.26	67.55	72.47	72.29	71.65	68.36	75.44	70.66	70.40	66.60	58.57	62.80	64.80
TiO ₂	0.95	1.00	0.86	1.77	1.27	1.12	1.15	0.90	0.97	1.18	0.64	0.62	1.00	0.78
Al ₂ O ₃	12.41	10.28	16.45	12.49	13.03	12.92	15.37	11.45	14.32	13.37	15.40	11.91	18.90	16.90
Fe ₂ O ₃	5.68	7.58	7.31	7.43	6.70	6.44	7.42	5.31	6.15	7.20	5.04	5.21	7.22	6.33
MnO	0.04	0.11	0.09	0.05	0.05	0.05	0.06	0.08	0.05	0.07	0.10	0.32	0.11	0.06
MgO	1.33	1.48	2.61	2.05	1.74	1.94	1.80	1.54	1.94	2.11	2.48	2.48	2.20	2.85
CaO	0.32	0.44	0.54	0.29	0.24	0.42	0.37	1.26	0.26	0.62	3.59	5.95	1.30	3.56
Na ₂ O	1.31	0.95	1.16	1.48	1.42	1.22	1.90	1.39	1.35	1.29	3.27	2.43	1.20	1.15
K ₂ O	2.29	1.67	3.08	1.84	2.55	2.32	2.41	1.83	2.66	2.58	2.80	2.04	3.70	3.99
P ₂ O ₅	0.12	0.28	0.11	0.15	0.10	0.12	0.23	0.12	0.12	0.10	0.15	0.19	0.16	0.11
SiO ₂ /Al ₂ O ₃	5.94	7.32	4.11	5.80	5.55	5.54	4.45	6.59	4.93	5.27	4.32	4.92	3.32	3.83
Al ₂ O ₃ /TiO ₂	13.06	10.28	19.22	7.06	10.28	11.52	13.33	12.68	14.78	11.34	24.06	19.21	18.90	21.67
K ₂ O/Al ₂ O ₃	0.18	0.16	0.19	0.15	0.20	0.18	0.16	0.16	0.19	0.19	0.18	0.17	0.20	0.24
K ₂ O/Na ₂ O	1.74	1.75	2.66	1.25	1.80	1.91	1.27	1.32	1.97	2.00	0.86	0.84	3.08	3.47
CIA	70.42	71.13	72.55	71.61	70.27	70.99	70.61	63.59	72.00	68.87	-	-	-	-
PIA	78.40	78.17	81.95	78.01	78.84	78.99	77.13	67.43	80.95	76.49	-	-	-	-
CIW	81.93	81.29	85.07	80.84	82.54	82.35	80.25	71.47	84.17	80.43	-	-	-	-
WIP	35.99	28.14	45.44	35.62	40.08	37.34	43.85	35.82	41.00	41.17	-	-	-	-
ICV	0.96	1.29	0.95	1.19	1.07	1.05	0.98	1.07	0.93	1.12	-	-	-	-
Sc	4.15	9.31	4.30	6.45	9.33	8.17	6.63	6.68	11.99	5.66	14.00	13.10	16.00	14.90
V	84.38	95.31	98.18	115.11	109.41	108.10	108.01	74.34	101.68	115.96	97.00	110.00	150.00	130.00
Cr	48.47	52.13	56.33	94.62	68.51	78.23	71.69	40.72	66.93	70.76	92.00	78.90	110.00	125.00
Co	13.33	12.30	15.54	17.21	17.02	13.81	14.84	10.23	14.91	17.54	17.30	21.90	23.00	25.70
Ni	25.16	32.41	33.42	33.83	33.09	32.65	38.00	23.54	33.20	36.39	47.00	70.50	55.00	58.00
Cu	19.54	30.49	22.59	25.76	23.78	24.75	34.23	20.18	21.49	25.97	28.00	75.00	50.00	-
Zn	21.57	21.48	24.92	41.35	25.24	20.99	34.03	25.72	26.87	25.94	67.00	86.40	85.00	-
Ga	14.26	13.34	15.65	16.92	17.14	15.13	16.54	12.00	16.59	16.11	-	-	-	-
Rb	75.88	62.09	102.79	63.61	98.99	78.63	81.38	58.24	110.35	84.66	82.00	57.20	160.00	125.00
Sr	42.81	58.04	55.88	44.05	64.44	63.47	65.79	60.83	87.56	59.16	320.00	327.00	200.00	142.00
Y	17.96	30.52	12.67	41.23	29.73	21.70	18.48	22.49	33.77	18.32	21.00	29.80	27.00	35.00
Zr	338.10	269.88	204.29	1323.98	445.35	425.25	289.28	298.22	339.97	393.87	193.00	130.00	210.00	200.00
Nb	18.43	16.98	14.57	30.28	21.90	20.45	19.02	16.50	18.82	20.80	12.00	8.94	19.00	13.00
Cs	2.68	3.14	5.28	2.84	3.87	3.47	3.60	2.37	6.36	3.20	-	-	-	-
Ba	239.41	260.11	318.92	206.98	353.94	359.58	376.28	203.91	400.67	314.90	628.00	776.00	650.00	636.00
Hf	10.48	8.55	6.57	40.68	14.27	13.55	9.41	9.33	10.79	12.69	-	-	-	-
Ta	1.54	1.40	1.23	2.52	1.44	1.78	1.53	1.21	1.54	1.70	-	-	-	-
Pb	4.91	4.41	6.17	16.25	12.13	11.93	22.66	4.25	12.01	22.47	17.00	19.90	20.00	-
Th	15.04	17.17	10.84	35.82	20.80	18.28	14.59	13.95	16.89	16.20	10.50	6.91	14.60	12.00

Table 3. (Continued.)

Oxides/elements	BS-16	BS-21	BS-25	BS-29	BS-36	BS-38	BS-46	BS-53	BS-54	BS-56	UCC	GLOSS	PAAS	NASC
U	2.56	2.22	2.06	6.78	3.25	2.90	3.68	2.38	2.68	3.01	2.70	1.68	3.10	2.66
Rb/Sr	1.77	1.07	1.84	1.44	1.54	1.24	1.24	0.96	1.26	1.43	0.26	0.17	0.80	0.88
Y/Ni	0.71	0.94	0.38	1.22	0.90	0.66	0.49	0.96	1.02	0.50	0.45	0.42	0.49	0.60
Co/Th	0.89	0.72	1.43	0.48	0.82	0.76	1.02	0.73	0.88	1.08	1.65	3.17	1.58	2.14
Th/Co	1.13	1.40	0.70	2.08	1.22	1.32	0.98	1.36	1.13	0.92	0.61	0.32	0.63	0.47
Cr/Th	3.22	3.04	5.20	2.64	3.29	4.28	4.91	2.92	3.96	4.37	8.76	11.42	7.53	10.42
Cr/Ni	1.93	1.61	1.69	2.80	2.07	2.40	1.89	1.73	2.02	1.94	1.96	1.12	2.00	2.16
Th/Cr	0.31	0.33	0.19	0.38	0.30	0.23	0.20	0.34	0.25	0.23	0.11	0.09	0.13	0.10
Zr/Cr	6.98	5.18	3.63	13.99	6.50	5.44	4.04	7.32	5.08	5.57	2.10	1.65	1.91	1.60
Th/Sc	3.63	1.84	2.52	5.56	2.23	2.24	2.20	2.09	1.41	2.86	0.75	0.53	0.91	0.81
Zr/Sc	81.51	28.98	47.47	205.32	47.72	52.07	43.65	44.62	28.36	69.62	13.79	9.92	13.13	13.42
Cr/V	0.57	0.55	0.57	0.82	0.63	0.72	0.66	0.55	0.66	0.61	0.95	0.72	0.73	0.96
Cr/Zr	0.14	0.19	0.28	0.07	0.15	0.18	0.25	0.14	0.20	0.18	0.48	0.61	0.52	0.63
Th/U	5.87	7.73	5.27	5.28	6.40	6.31	3.96	5.85	0.00	5.38	3.89	4.11	4.71	4.51
La	43.04	39.01	24.24	79.92	55.32	44.14	36.73	35.62	48.23	40.44	31.00	28.80	38.20	31.10
Ce	90.44	81.06	54.03	169.36	119.32	93.21	75.40	74.10	97.53	86.36	63.00	57.30	79.60	67.03
Pr	10.82	9.65	6.36	19.97	14.01	11.00	9.38	8.82	11.64	10.62	7.10	-	8.83	-
Nd	40.28	36.21	24.21	73.53	52.58	39.86	34.52	31.86	43.06	39.61	27.00	27.00	33.90	30.40
Sm	7.72	7.52	4.61	14.01	10.15	7.48	6.68	6.23	8.52	7.47	4.70	5.78	5.55	5.98
Eu	1.48	1.66	0.94	2.44	2.03	1.39	1.32	1.22	1.74	1.39	1.00	1.31	1.08	1.25
Gd	5.99	6.94	3.75	11.60	8.25	5.67	5.45	5.16	7.19	5.58	4.00	5.26	4.66	5.50
Tb	0.92	1.17	0.61	1.81	1.31	0.94	0.88	0.85	1.19	0.89	0.70	-	0.77	0.85
Dy	4.48	6.25	3.14	9.22	6.67	4.90	4.47	4.52	6.53	4.42	3.90	4.99	4.68	5.54
Ho	0.87	1.26	0.64	1.87	1.34	1.02	0.91	0.95	1.35	0.91	0.83	-	0.99	-
Er	2.31	3.46	1.77	5.22	3.68	2.93	2.47	2.69	3.84	2.54	2.30	2.92	2.85	3.28
Tm	0.29	0.45	0.23	0.69	0.48	0.40	0.32	0.36	0.52	0.34	0.30	-	0.41	-
Yb	1.83	2.94	1.51	4.65	3.21	2.77	2.00	2.45	3.55	2.27	2.00	2.76	2.82	3.11
Lu	0.27	0.43	0.22	0.68	0.47	0.40	0.29	0.36	0.52	0.33	0.31	0.41	0.43	0.46
(La/Yb) _N	15.89	8.97	10.83	11.61	11.65	10.79	12.43	9.82	9.19	12.06	10.47	7.05	9.15	6.75
(La/Sm) _N	3.51	3.26	3.31	3.59	3.43	3.72	3.46	3.60	3.56	3.41	4.15	3.14	4.33	3.27
(Gd/Yb) _N	2.65	1.91	2.01	2.02	2.08	1.66	2.21	1.71	1.64	2.00	1.62	1.54	1.34	1.43
Eu/Eu*	0.64	0.69	0.67	0.57	0.66	0.63	0.65	0.64	0.66	0.63	0.69	0.71	0.63	0.66
(La/Lu) _N	16.76	9.45	11.42	12.25	12.28	11.37	13.11	10.36	9.69	12.72	10.38	7.24	9.22	7.08
LOI	2.97	3.34	4.13	1.6	2.43	3.06	4.73	2.67	2.89	2.83	-	-	-	-

Note. CIA: Chemical Index of Alteration after Nesbitt and Young (1982), PIA: Plagioclase Index of Alteration after Fedo *et al.* (1995), CIW: Chemical Index of Weathering after Harnois (1988), WIP: Weathering Index of Parker (1970), ICV: Index of Chemical Variability after Cox *et al.* (1995), UCC: Upper Continental Crust after Rudnick and Gao (2003), GLOSS: Global Subducting Sediment after Plank and Langmuir (1998), PAAS: Post-Archean Australian Shales after Taylor and McLennan (1985), NASC: North American Shale Composite after Gromet *et al.* (1984).

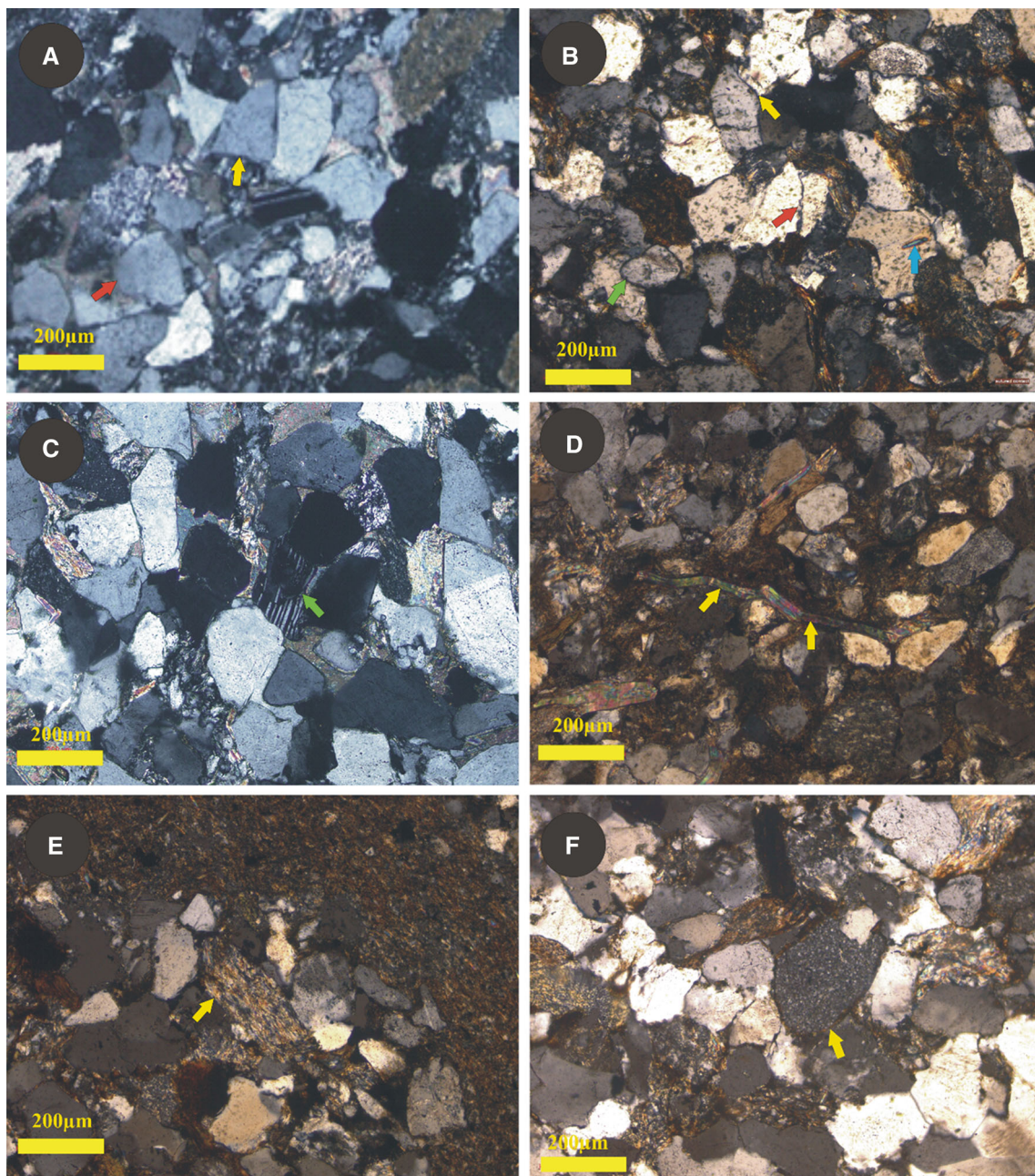


Figure 4. Photomicrographs of Barail Sandstones showing monocrystalline quartz of subangular (yellow arrow) and subrounded (red arrow) shape (A), long (yellow arrow), concavo-convex (green arrow) and sutured (red arrow) contacts and inclusion of heavy minerals (blue arrow) in monocrystalline quartz (B), fractured plagioclase (green arrow) with gneissic rock fragment (red arrow) (C), mica mineral showing a kink bend (yellow arrow) due to compaction effect (D), metamorphic (schist) rock fragment (yellow arrow) (E), chert grain (yellow arrow) cemented in siliceous cement (F). All photomicrographs were taken under $\times 20$ magnification.

cement can be attributed to compaction of sandstone, thereby causing pressure solution, which is the most important indigenous source of silica. The quartz overgrowth (figure 5C) present in the sandstones may be the intra-formational release of silica during replacement and corrosion of feldspar and mica by calcite. Besides silica cement, iron oxide and calcite cement are also observed in the

Barail Sandstones. Iron oxide cement occurs as a dark black coating on the detrital quartz and feldspar grains as well as scattered aggregates and pervasive pore fillings. Carbonate cement has replaceable relationship with quartz and feldspar. Floating grains with corroded boundaries may be attributed to replacement of framework grains by cementing materials (figure 5D). The petrographic

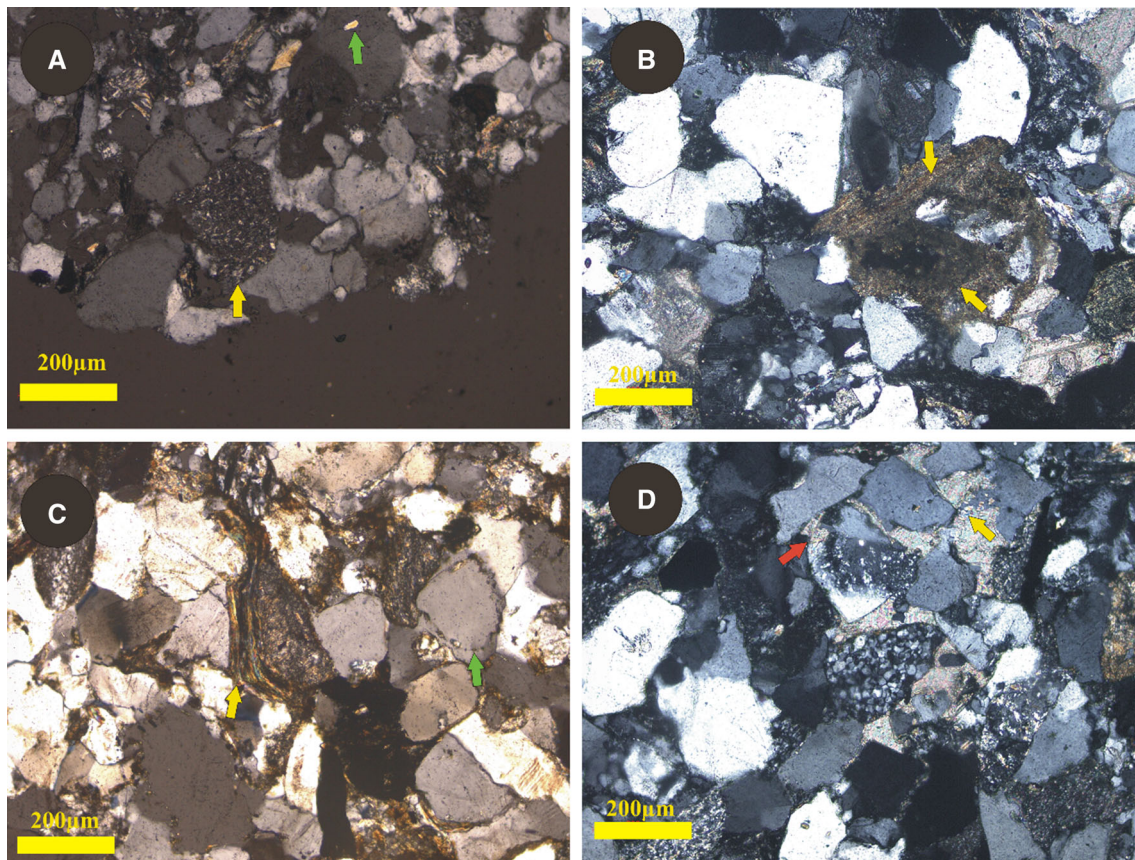


Figure 5. Photomicrographs of Barail Sandstone showing volcanic rock fragment (yellow arrow) and inclusion of heavy mineral (green arrow) in monocrystalline quartz (A), pseudomatrix (yellow arrow) formed due to compaction of weaker sedimentary rock fragments (B), pseudomatrix (yellow arrow) formed from low grade metamorphic rock fragments and quartz overgrowth (green arrow) (C), floating texture (yellow arrow) and peripheral dissolution (red arrow) of quartz by calcareous cement (D). All photomicrographs were taken under $\times 20$ magnification.

study also reveals the presence of several diagenetic features such as corrosion, oversized pores and complete replacement of detrital grains by carbonate cement. The quartz, feldspar and rock fragment grains are recalculated to 100 (table 2) and the data are plotted in QFR plot (Folk 1980), which infers that the Barail Sandstones are mainly subarkosic and less commonly of sublitharenite types.

4.2 Geochemistry of Barail Sandstones

4.2.1 Major elements

The major element analyses for the Barail sandstones are presented in table 3. The studied sandstones have high concentration of SiO_2 ranging between 67.55 and 75.44 wt.% and display a sharp negative correlation with Al_2O_3 ($R = -0.96$). This implies differentiation of clay and quartz during the sedimentation processes. Similarly, CaO ($R = -0.24$), MnO ($R = -0.25$), P_2O_5 ($R = -0.30$) and

TiO_2 ($R = -0.13$) are negatively correlated with Al_2O_3 (figure 6). But Na_2O ($R=0.40$), MgO ($R = 0.73$), K_2O ($R = 0.87$), Fe_2O_3 ($R = 0.25$) show a positive correlation with Al_2O_3 . Fe_2O_3 ($R = 0.43$) shows a moderate positive correlation with TiO_2 (figure 6). The enrichment of both the elements in sediments (avg. Fe_2O_3 : 6.72 wt.%, TiO_2 : 1.12 wt.%) indicate the presence of Fe and Ti bearing heavy minerals, cements and mark their association with clay minerals. Various diagenetic processes lead to the enrichment of Fe_2O_3 during sedimentation processes. The positive correlation of Na_2O , MgO , K_2O and Fe_2O_3 with Al_2O_3 (figure 6) also indicate the presence of these elements with clay minerals and with the rock fragments. The ratio of $\text{SiO}_2/\text{Al}_2\text{O}_3$ (avg. 5.55) is high indicating influence of recycling processes, weathering and sediment transport. Quartz population increases simultaneously along with these processes. The concentrations of the elements are almost similar with the Upper Continental Crust (UCC, Taylor and McLennan 1985). The higher

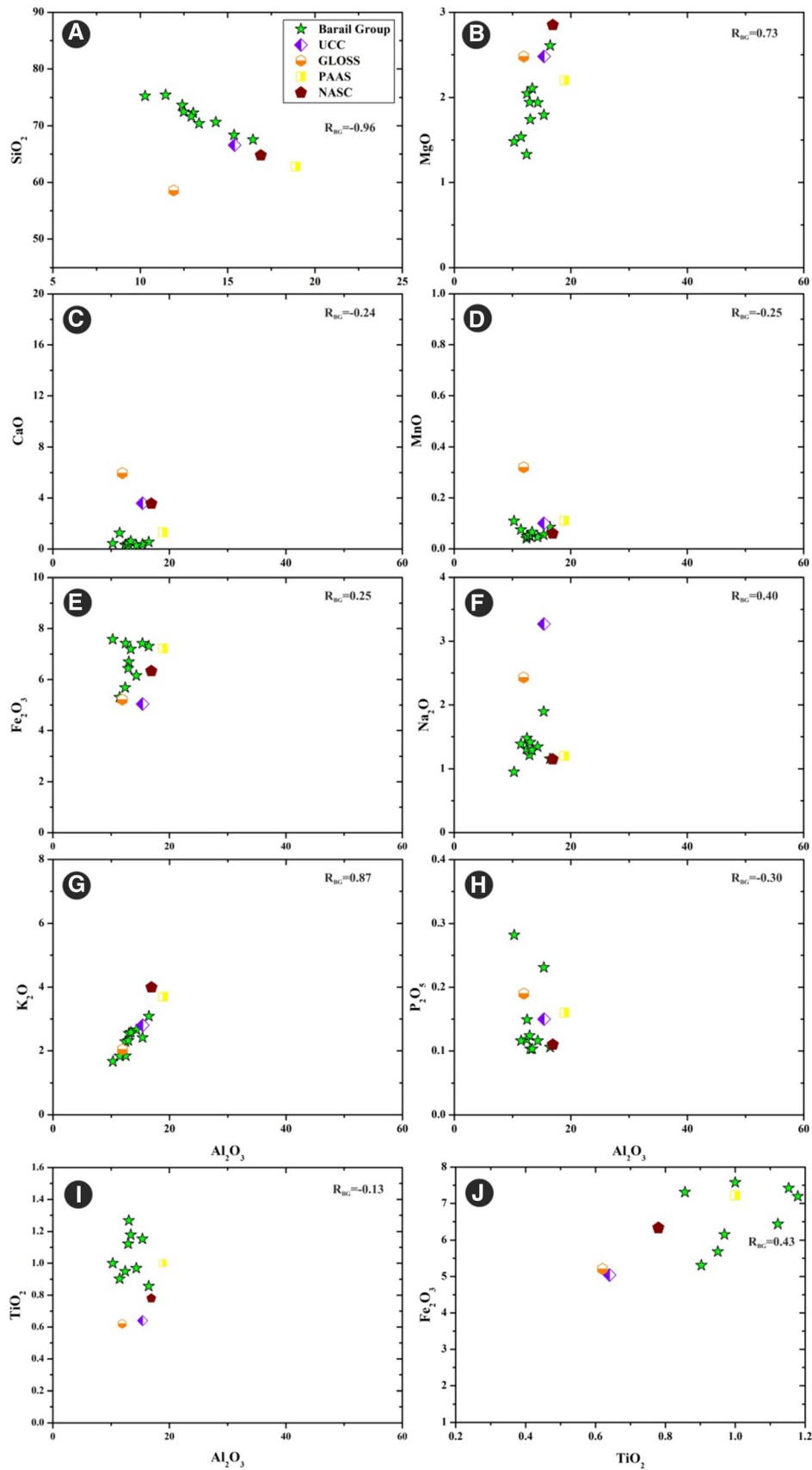


Figure 6. Al_2O_3 vs. major oxides covariation diagram (A–I), correlation between Fe_2O_3 and TiO_2 for the Barail Sandstones (J).

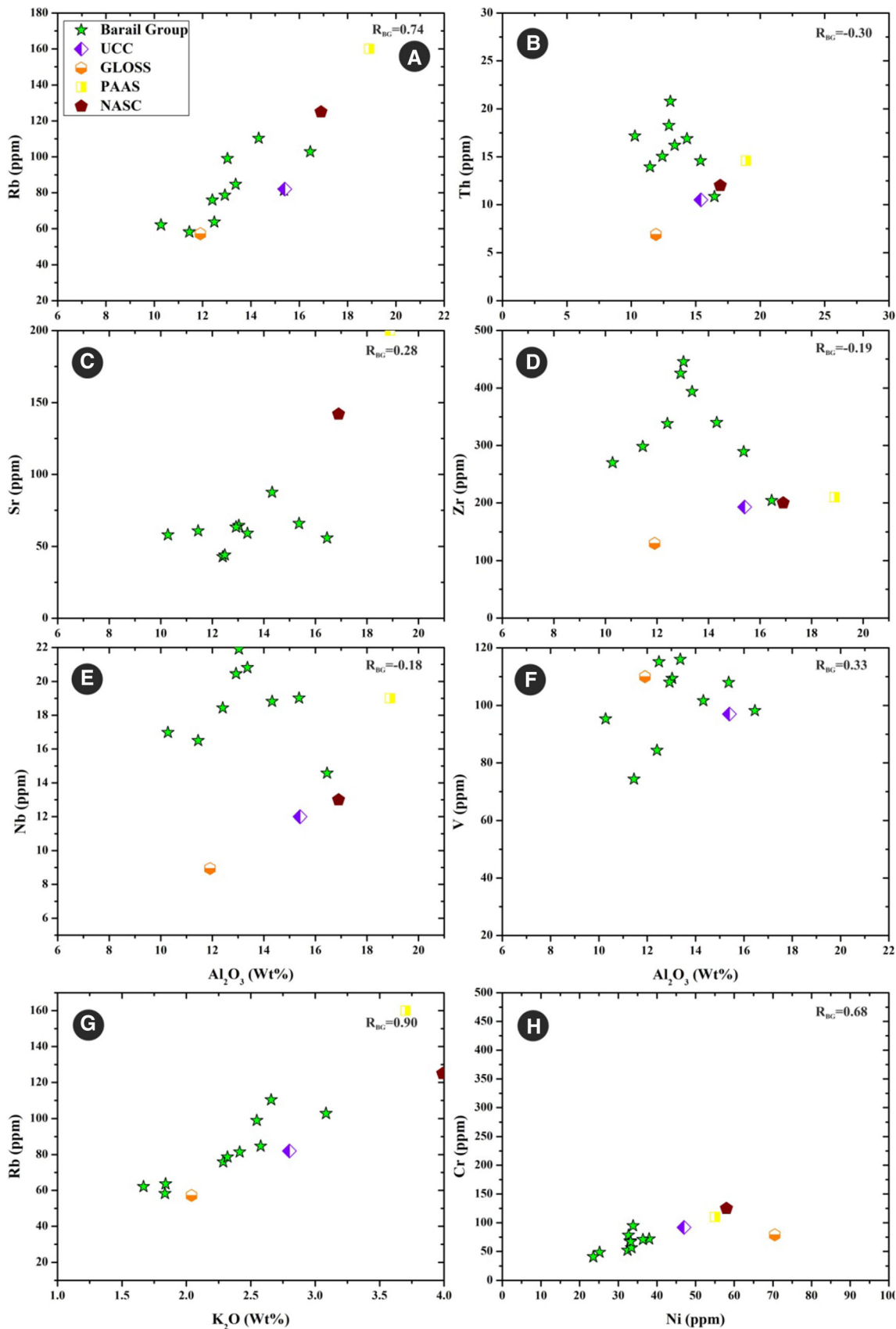


Figure 7. Al_2O_3 vs. trace elements covariation diagram (A–F); correlation between Rb and K_2O (G) and Ni vs. Cr (H) for the Barail Sandstones.

ratio of Al_2O_3/TiO_2 (avg. 12.35) indicates the probable continental derivation of the sediments (Fyffe and Pickerill 1993). The UCC (Taylor and McLennan 1985) normalized (figure 8A) pattern of oxides of the samples show depletion of CaO, Na_2O , MgO and K_2O .

4.2.2 Trace elements

Among the various trace elements, LILE are depleted (avg. Sr: 60.20 ppm, Ba: 303.47 ppm); HFSE are enriched (avg. Zr: 432.82 ppm, Nb: 19.77 ppm, Hf: 13.63 ppm, Th: 17.96 ppm, U: 3.15 ppm, Ta: 1.59 ppm) and transitional elements are also depleted (avg. Sc: 7.27 ppm, Cr: 64.84 ppm, Co: 14.67 ppm, Ni: 32.17 ppm, Cu: 24.88 ppm, Zn: 26.81 ppm; except Y: 24.69 ppm and V: 101.05 ppm) compared to the UCC (Taylor and McLennan 1985). Rb ($R = 0.74$), V ($R = 0.33$) and Sr ($R = 0.28$) are showing positive correlation with Al_2O_3 (figure 7) which indicates the association of these elements with the clay minerals like illite, chlorite, kaolinite, etc. While trace elements Zr ($R = -0.19$), Th ($R = -0.30$) and Nb ($R = -0.18$) shows a negative correlation with Al_2O_3 . Concentration of Zr is higher (avg. 432.82 ppm) due to its detrital association with zircons. The high concentration of Rb (avg. 81.66 ppm) is due to the presence of K bearing clay minerals like kaolinite, illite, etc. It is showing a sharp positive correlation with K_2O ($R=0.90$). The concentrations of the various trace elements in terms of ppm are given in table 3 and UCC (Taylor and McLennan 1985) normalized pattern of trace elements are presented in figure 8(B).

4.2.3 Rare earth elements

The concentration of REE along with certain elemental ratios of Barail Sandstones are represented in table 3. The chondrite (Taylor and McLennan 1985) normalized REE pattern (figure 8C) shows an enrichment of light rare earth elements (LREE: La–Gd), depleted heavy rare earth elements (HREE: Tb–Lu) along with a negative Eu anomaly. The ratio of $(La/Yb)_N$ is (8.97–15.89) is comparatively higher when compared with the UCC: 10.47 (Taylor and McLennan 1985). $Eu/Eu^* = 0.57–0.69$, $(La/Sm)_N = 3.26–3.72$ and $(Gd/Yb)_N = 1.64–2.65$ ratio bears resemblance with the characteristics of UCC (Taylor and McLennan 1985). The HREE pattern (figure 8C) indicates a depleted

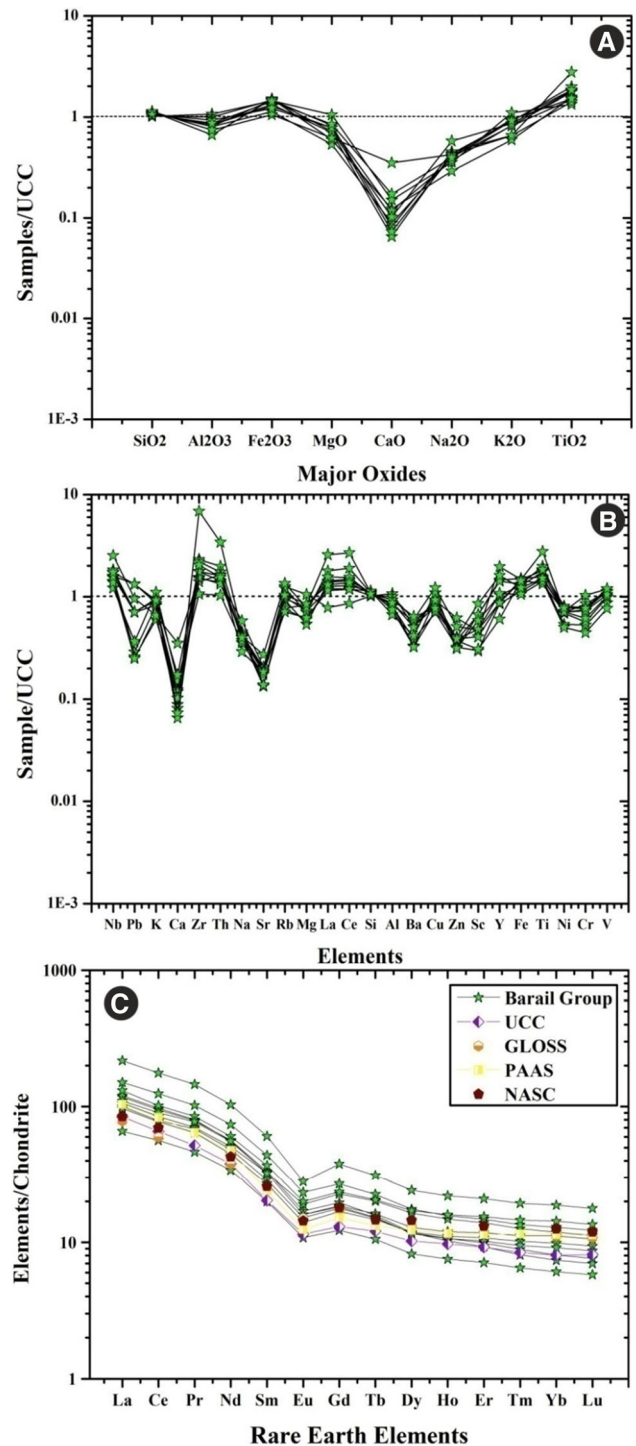


Figure 8. (A) UCC normalized compositional plot for major oxides; (B) UCC normalized multi-element plot and (C) Chondrite normalized REE patterns for the Barail sandstones.

source which is represented by higher ratio of $(Gd/Yb)_N =$ (avg. 1.99). Also the higher ratio of $(La/Lu)_N =$ (9.45–16.76) indicates a fractionated source rock of upper crustal signature which is a typical pattern shown by fractionated granitoids.

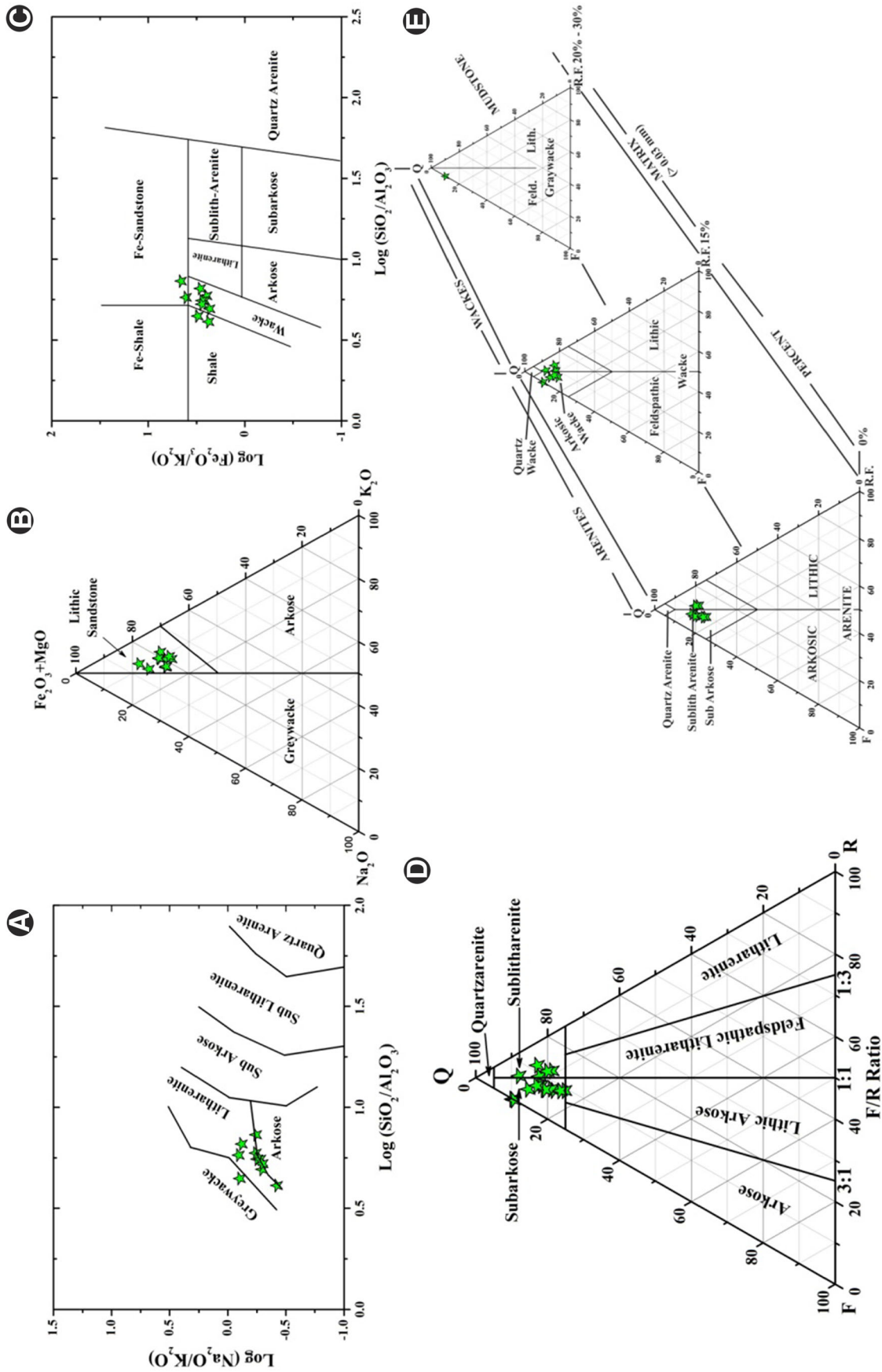


Figure 9. Classification of Barail sandstones. (A) Sand scheme classification after Pettijohn and Siever (1972); (B) Sand scheme classification after Blatt *et al.* (1980); (C) Geochemical classification after Herron (1988); (D) Detrital classification after Folk (1980), and (E) petrographical classification after Pettijohn *et al.* (1972).

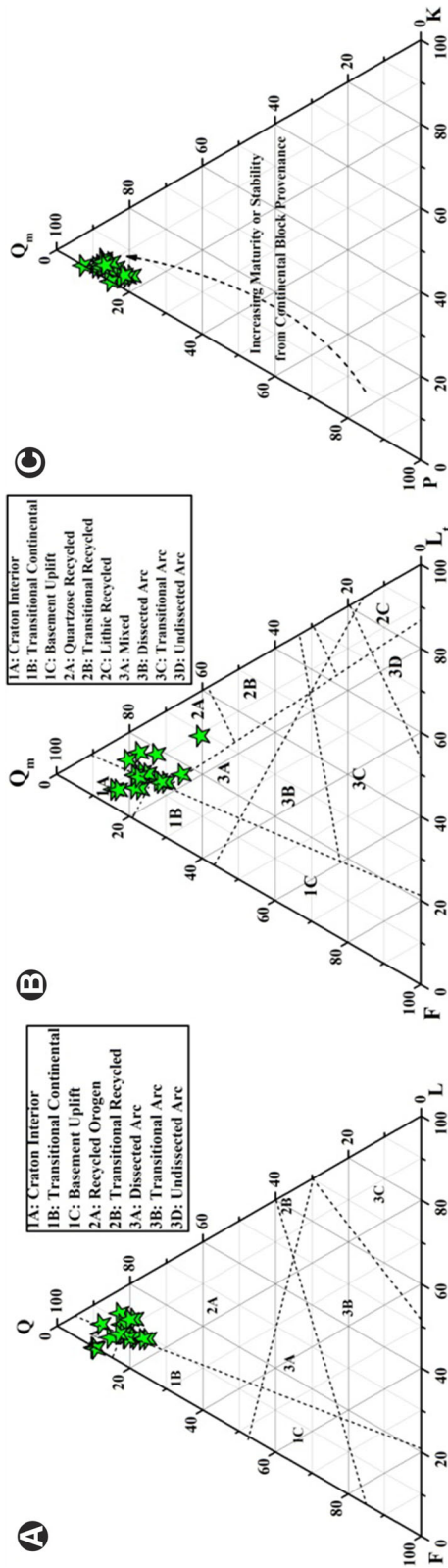


Figure 10. Tectonic discrimination plot. (A) Q–F–L ternary plot after Dickinson and Suczek (1979); (B) Q_m –F– L_t ternary plot after Dickinson *et al.* (1983), and (C) Q_m –P–K ternary plot after Dickinson (1985) of Barail Sandstones.

4.3 Sandstone classification

Major elemental concentrations are used for classification of the various types of sandstones (Pettijohn *et al.* 1972; Blatt *et al.* 1980; Herron 1988). In the classification scheme after Pettijohn *et al.* (1972), the logarithmic values of ratio of (SiO_2/Al_2O_3) vs. (Na_2O/K_2O) are used, where most of the samples appear litharenitic type (figure 9A). Blatt *et al.* (1980) introduced another sand scheme classification in the form of a ternary plot by using the wt.% values of Na_2O , (Fe_2O_3+MgO) and K_2O to classify sandstones into greywacke, arkose and lithic sandstone types in which the studied samples plot confined within the field of lithic sandstone (figure 9B). Herron (1988) used the logarithmic values of ratio of (SiO_2/Al_2O_3) vs. (Fe_2O_3/K_2O) to classify sandstones basically into Fe-rich (Fe-shale and Fe-sandstone) and Fe-poor (shale, wacke, litharenite and arkose). In the plot (figure 9C), most of the Barail Sandstone are classified as wacke. Again, as per the detrital scheme of sandstone classification proposed by Folk (1980), the sandstones are mostly subarkosic type followed by sublitharenite (figure 9D). Dott’s classification scheme after Pettijohn *et al.* (1972) shows subarkosic to arkosic wacke type sandstone followed by sublitharenite to lithic greywacke (figure 9E).

5. Discussion

5.1 Tectono-provenance

The modal data and the Q–F–L and Q_m –F– L_t plots (Dickinson 1983) in figure 10(A, B) for the studied sandstones clearly indicate a recycled orogen provenance with subordinate contribution from craton interior. The Q_m –P–K ternary plot after Dickinson (1985) shows the derivation of sediments from continental block provenance (figure 10C). Within recycled orogens, the sediments are derived dominantly from sedimentary and metamorphic rocks exposed to erosion by orogenic uplift of fold belts and thrust sheets (Dickinson and Suczek 1979; Dickinson 1983). In the present study, the dominance of metamorphic and sedimentary rock fragments indicates the derivation of the sediments from recycled orogen sources. Basu *et al.* (1975) pointed out that undulose extinction and polycrystallinity of quartz grains can be used for reliable interpretation of provenance. He also demonstrated that low rank metamorphic rocks

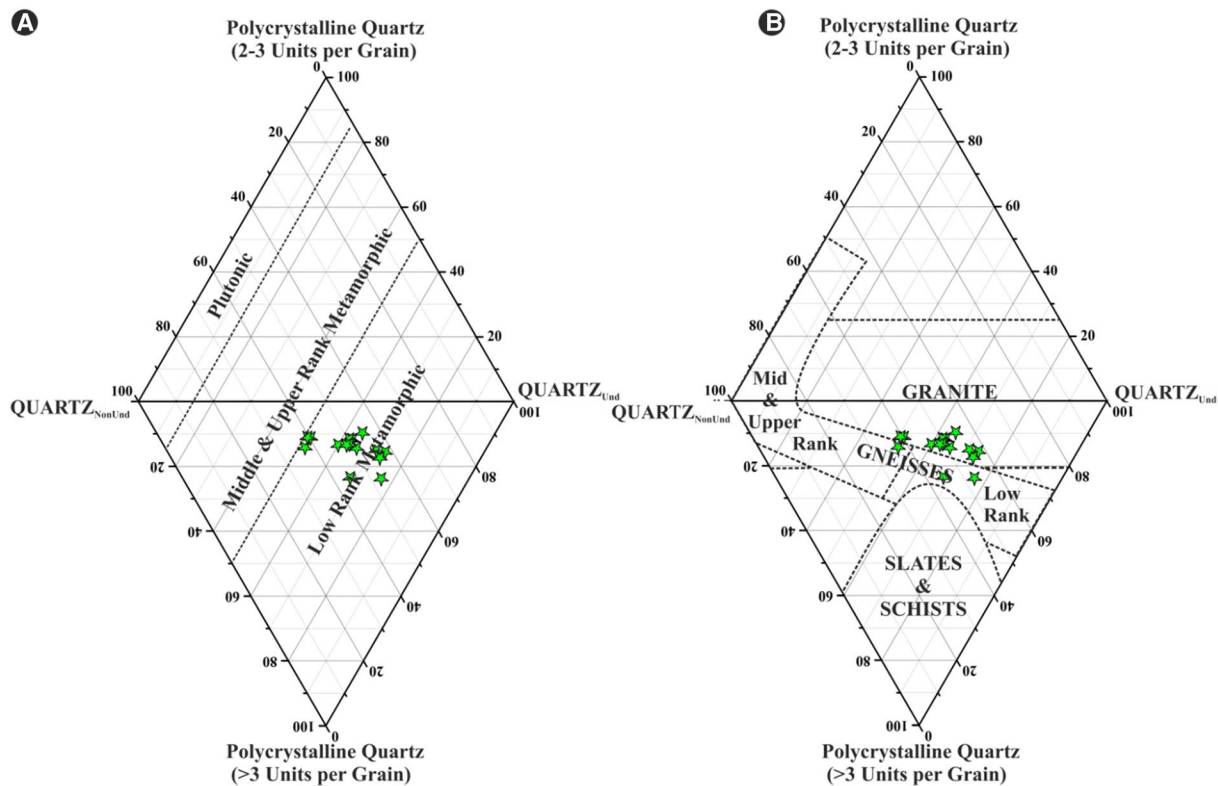


Figure 11. (A) Diamond plot after Basu *et al.* (1975) of Barail sandstones representing their derivation from low rank metamorphics and (B) modified diamond plot after Tortosa *et al.* (1991) representing derivation of sediments from granite and gneisses.

contain large amount of quartz with more than three crystals per grain and contain both undulose and non-undulose quartz, whereas plutonic quartz is predominantly non-undulose and monocrystalline. Dominance of polycrystalline quartz in the studied sandstones indicates their derivation from low grade metamorphic rocks. This is also reflected in diamond diagram plot (Basu *et al.* 1975) in figure 11(A). Folk (1980) opined that quartz grains with undulatory extinction are weaker because they have been plastically deformed. He concluded that assemblages of quartz grains that have spent more time in the sedimentary environment should be relatively enriched in non-undulatory monocrystalline grains and depleted in undulatory polycrystalline grains, i.e., the more the maturity of the sandstones, the more the non-undulatory quartz and the less polycrystalline grains. The presence of straight to slightly undulose monocrystalline quartz (avg. 18.70%) in the studied sandstones suggests a common plutonic source. The diamond plot after Tortosa *et al.* (1991) (figure 11B), also suggests granitic sources for the sediments.

Trace and rare earth elements are generally insensitive to the sedimentation processes. Certain

trace and REE ratios are helpful for the prediction of source rock for clastic sedimentary rocks. The standard values of certain elemental ratios of trace and rare earth elements as proposed by Cullers (1994, 2000) and Cullers and Podkovyrov (2002) against different sources are presented in table 4. The ranges of these elemental ratios shown by Barail Sandstones are: La/Sc: 4.02–12.39, La/Co: 1.55–4.64, Th/Sc: 1.41–5.55 and Cr/Th: 2.64–5.19. These values represent the contribution of sediments from felsic source rocks. Moreover, incompatible ferromagnesian trace elements like Ni, Cr, V, and Sc are considerably low to moderate indicating the source as felsic.

Because of the immobile nature of trace elements during the sedimentation processes, the ternary plot of V–Ni–Th \times 10 after Bracciali *et al.* (2007) is often used to identify the source rocks. Trace elements, viz., V and Ni are commonly concentrated in the mafic and ultramafic rocks, but concentration of Th is found mostly in the felsic rocks. From the plot (figure 12A) after Bracciali *et al.* (2007), it is observed that the Barail sandstones are rich in Th, moderate concentration of V, while depleted in Ni. Hence most of the samples are confined near to the felsic field in the plot. Hayashi *et al.* (1997)

Table 4. Table showing certain Trace and REE elemental ratios representing provenance (felsic and mafic sources are after Cullers 1994, 2000 and Cullers and Podkovyrov 2002).

Elemental ratio	Range of Barail						
	Sandstone	Felsic sources	Mafic sources	UCC	GLOSS	PAAS	NASC
Eu/Eu*	0.57–0.69	0.32–0.83	0.70–1.02	0.69	0.71	0.63	0.65
La/Lu	9.45–16.76	3.00–27.0	1.10–7.00	10.38	7.24	9.22	7.08
La/Sc	4.02–12.39	0.70–27.7	0.40–1.1	2.21	2.2	2.39	2.09
La/Co	1.56–4.64	1.4–22.4	0.14–0.38	1.79	1.31	1.66	1.21
Th/Sc	1.41–5.55	0.64–18.1	0.05–0.4	0.75	0.53	0.91	0.8
Th/Co	0.69–2.08	0.30–7.5	0.04–1.40	0.6	0.31	0.63	0.46
Cr/Th	2.64–5.19	4.00–15.0	25–500	8.76	11.42	7.53	10.41
Th/Cr	0.19–0.38	0.06–4.0	0.002–0.045	0.11	0.09	0.13	0.1

proposed that TiO_2/Zr ratio decreases with the increasing concentration of SiO_2 and suggests that the ratio of TiO_2/Zr is $> \sim 200$ for mafic source, 195–55 for intermediate source and < 55 for felsic source rock for clastic sediments. The ratio of TiO_2/Zr (13.35–41.90; avg. 30.38) of the Barail sandstones suggests its derivation from the felsic source (figure 12B). McLennan *et al.* (1993) proposed the Zr/Sc *vs.* Th/Sc bivariate plot (figure 12C) to check the source composition and effects on source by sedimentation processes. In that plot, the straight trend represents the original source rock composition and the diversion trend represents the effect of sedimentation processes. Few of the samples plot along the straight trend indicating the original source rock composition, derived from felsic rocks while others are following a diversion trend representing the effects on the source rocks due to sedimentation processes (figure 12C).

Floyd and Leveridge (1987) reported that sediments sourced from the acidic arcs generally exhibits low ratio of La/Th along with moderate range of Hf (3–7 ppm). In the binary plot of Hf *vs.* La/Th after Floyd and Leveridge (1987) (figure 12D), the studied sandstones show moderate ratio of La/Th with enrichment of Hf (avg. 13.60 ppm) suggesting the sediments were sourced from recycled sediments which were originally derived from arc-related acidic source rocks. This result is also supported by the binary plot of Zr/Sc *vs.* Th/Sc of McLennan *et al.* (1993) (figure 12C) which shows the recycled nature of Barail sediments with considerably higher concentration of Zr. It may therefore be inferred that the sediments are derived from the acidic arcs of Himalayan and Indo-Burmese ranges and recycling sediments generated from these arc related granitoids. In the

surrounding orogens of the studied rocks, there are presence of acidic arc related rocks primarily granitoids and their metamorphic equivalents (Ahmad *et al.* 2008; Reichardt *et al.* 2010; Zeng *et al.* 2014; Jiang *et al.* 2015; Gardiner *et al.* 2017; Xu *et al.* 2017). Some remarkable granitic terrain of these tectonic domain includes the northerly located Tangtse Pluton (Reichardt *et al.* 2010), Shyok Valley (Reichardt *et al.* 2010), Karakoram Batholith (Reichardt *et al.* 2010); Yangbajin Granite (Ahmad *et al.* 2008); Ladakh Granite (Ahmad *et al.* 2008); Yardo Dom (Zeng *et al.* 2014); Dala Granite (Zeng *et al.* 2014); Raidang Leucogranite (Zeng *et al.* 2014); Yardo Leucogranite (Zeng *et al.* 2014); Jirong Batholith (Jiang *et al.* 2015); Chikang Batholith (Jiang *et al.* 2015), etc., and easterly located Banmauk (Gardiner *et al.* 2017); Wuntho (Gardiner *et al.* 2017); Monywa (Gardiner *et al.* 2017); Myitkyina Plagiogranite (Xu *et al.* 2017), etc.

The chondrite (Taylor and McLennan 1985) normalized REE patterns and Eu anomaly give clues to the nature of source rocks (Basu *et al.* 1975; Armstrong-Altrin 2009). Felsic rocks show a higher LREE/HREE ratio and negative Eu anomalies (Cullers 1994, 2000). From the plot (figure 8C), it is evident that the concentration of LREE is extremely high as compared to HREE. The higher LREE/HREE ratio along with negative Eu anomaly indicates derivation of the clastic sediments from granitoids and/or its metamorphic equivalents. It represents a post-Archean source which is also supported by enrichment of K. The negative Eu anomaly is due to the fractionation of Ca-rich plagioclase from the source rocks. The concentration of Sr is also remarkably less (avg. 60.20 ppm) and thus supports the removal of Ca-rich plagioclase.

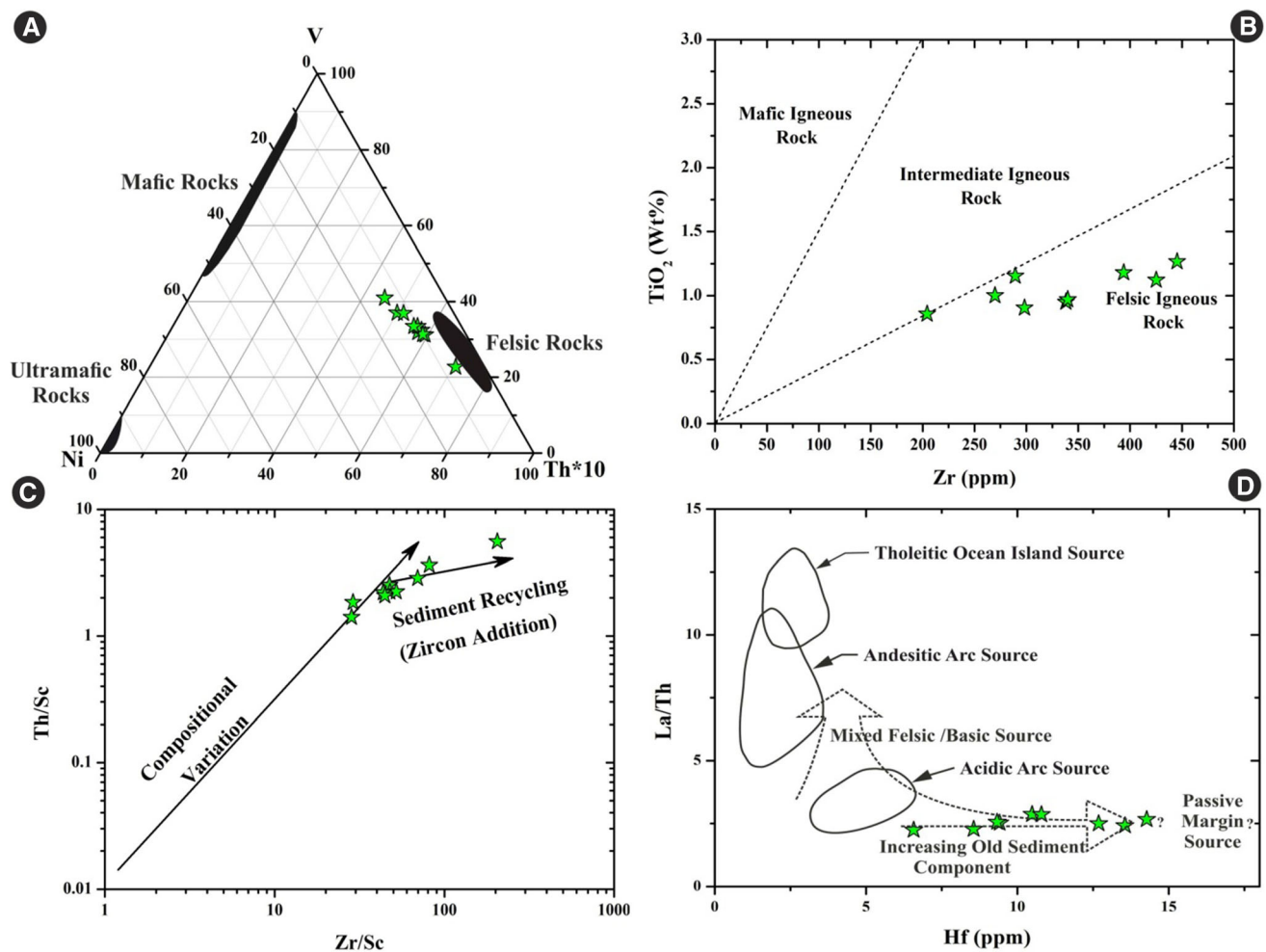


Figure 12. (A) Provenance ternary plot of V–Ni–Th \times 10 after Bracciali *et al.* (2007); (B) Zr vs. TiO₂ bivariate plot showing the possible source rocks for Barail Group after Hayashi *et al.* (1997); (C) Zr/Sc vs. Th/Sc binary plot after McLennan and Hanson (1993) representing the original source composition along with extent of sediment recycling, and (D) Hf vs. La/Th binary plot after Floyd and Leveridge (1987) representing derivation of sediments from acidic source.

Considering the proportions of different oxides in sands of various tectonic settings as proposed by Bhatia (1983), the studied sandstones indicate their derivation from active continental margin as well as oceanic island arc settings. Abundance of SiO₂ (avg. 71.50%) and Al₂O₃/SiO₂ (avg. 0.18) indicates active continental, while Fe₂O₃ + MgO (avg. 8.57 wt.%), TiO₂ (1.17) suggests oceanic island arc setting. The binary plot of (Fe₂O₃ + MgO) vs. TiO₂ (figure 13A) shows majority of the sample clusters in the field of oceanic island arc. This is because at the beginning of the collision between the Indian plate and the Burmese plate, the oceanic part of both plates collided and many granitoids have been emplaced in an arc setting. Bivariate plot of La/Sc vs. Ti/Zr (figure 13B) after Bhatia and Crook (1986) indicates the tectonic setting as active continental

margin with a suggested ratio of La/Sc: 3–6 (avg. Barail sandstones – La/Sc: 6.59). Moreover, the binary plot of discriminant function: DF-1: $[(-0.0447 \times \text{SiO}_2) - (0.972 \times \text{TiO}_2) + (0.008 \times \text{Al}_2\text{O}_3) - (0.267 \times \text{Fe}_2\text{O}_3) + (0.208 \times \text{FeO})(3.082 \times \text{MnO}) + (0.14 \times \text{MgO}) + (0.195 \times \text{CaO}) + (0.719 \times \text{Na}_2\text{O}) - (0.032 \times \text{K}_2\text{O}) + (7.51 \times \text{P}_2\text{O}_5) + 0.303]$ and DF-2: $[(-0.421 \times \text{SiO}_2) + (1.988 \times \text{TiO}_2) - (0.526 \times \text{Al}_2\text{O}_3) - (0.551 \times \text{Fe}_2\text{O}_3) - (1.61 \times \text{FeO}) + (2.72 \times \text{MnO}) + (0.881 \times \text{MgO}) - (0.907 \times \text{CaO}) - (0.177 \times \text{Na}_2\text{O}) - (1.84 \times \text{K}_2\text{O}) + (7.244 \times \text{P}_2\text{O}_5) + 43.57]$ after Bhatia (1983) (figure 13C) represents an active continental marginal setting for the studied sandstones. The ternary plot of La–Th–Sc after Bhatia (1983) (figure 13D) also suggests an active continental margin setup for the studied sandstones.

Hossain *et al.* (2010) also noted that the Barail and Surma Group sandstones of northeast Bengal

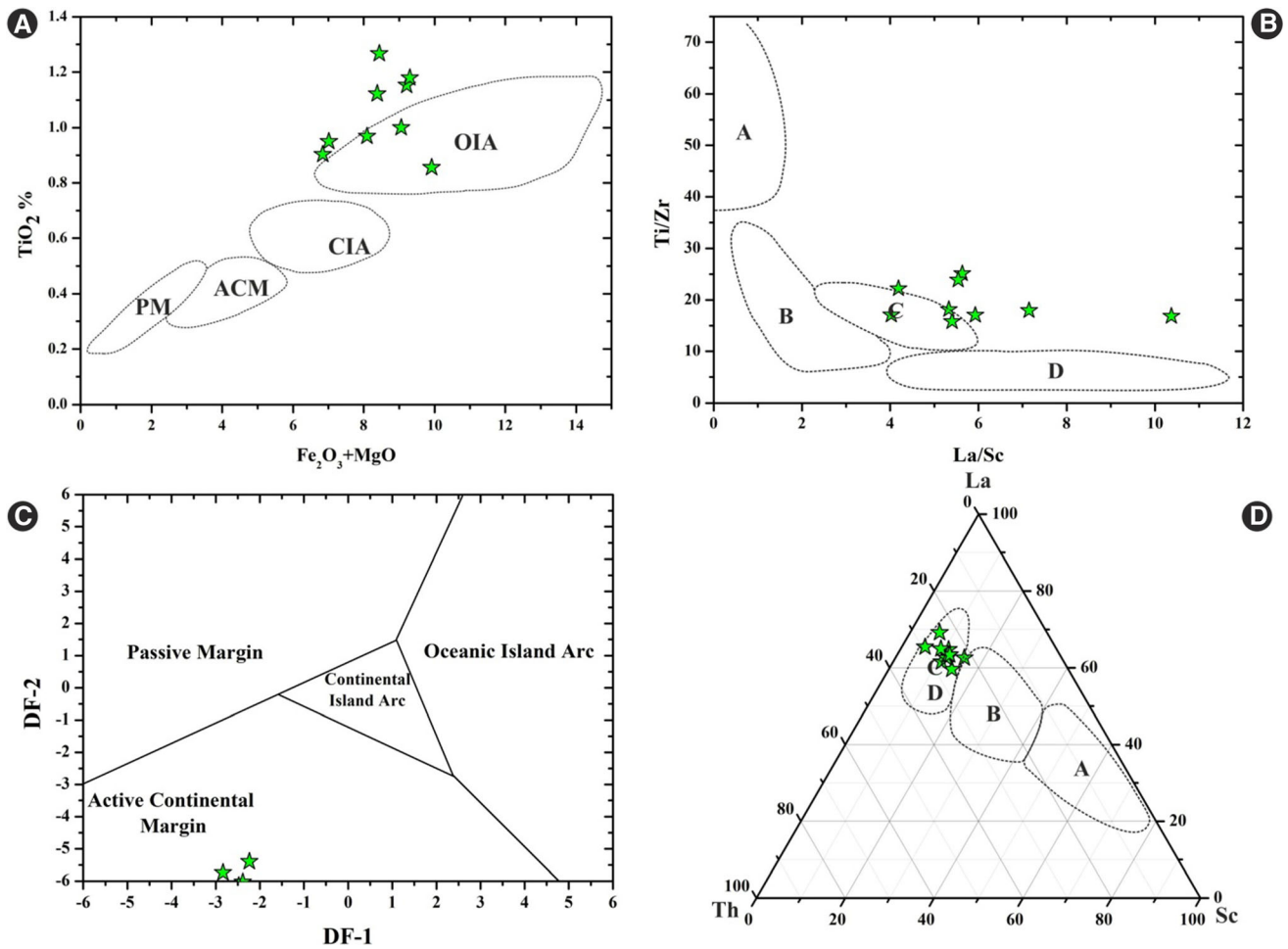


Figure 13. Tectonic discrimination plot. (A) $(Fe_2O_3 + MgO)$ vs. TiO_2 plot after Bhatia (1983); (B) La/Sc vs. Ti/Zr plot after Bhatia and Crook (1986), where A: Oceanic Island Arc, B: Continental Island Arc, C: Active Continental Margin and D: Passive Margin. (C) Discriminant function plot after Bhatia (1983), and (D) Th–La–Sc discrimination plot after Bhatia (1983) of Barail sandstones.

Basin, Bangladesh are quartz-rich, feldspar-poor, have lithic fragment population dominated by sedimentary and metamorphic clasts and were derived from a recycled orogen. Previous studies made by Uddin and Lundberg (1998) also forwarded the same conclusion and noted that the Barail sandstones were derived from proto-Himalayan sources. Najman and Garzanti (2000) suggested derivation of both the Barail and Surma Groups from early Himalayan thrust sheets. The overall results of the present study show that the studied sandstones were derived mainly from recycled orogen sources with subordinate contribution from oceanic island arc and active continental marginal settings. The sediments were derived from the uplifted and eroded Himalayan crystalline felsic terrain. Moreover, contribution from the near-most eastern orogen, i.e., Indo-

Burmese Ranges along with their recycled sediments cannot be ruled out.

5.2 Provenance mixing model

Trace and REEs are helpful for the prediction of source rock from where the sediments were derived (Mongelli *et al.* 2006; Schoenborn and Fedo 2011). The chondrite (Taylor and McLennan 1985) normalized REE pattern and Sc vs. Th/Sc binary plot after Schoenborn and Fedo (2011) are used for the quantitative estimation of source rock. Barail sandstones are showing an average ratio of $Th/Sc = 2.66$, which resembles with the mixing model Th/Sc ratio (1.15). Similarly chondrite (Taylor and McLennan 1985) normalized REE pattern also resembles with the REE pattern of mixing trend after Schoenborn and Fedo (2011). REE itself

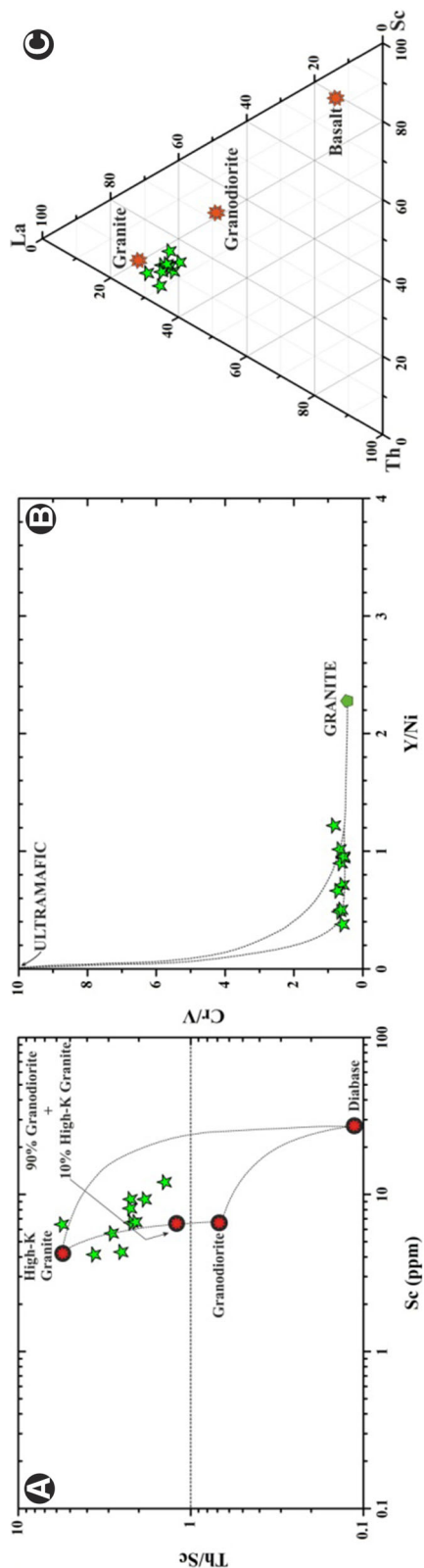


Figure 14. Provenance mixing plot. (A) Sc vs. Th/Sc plot for Barail Sandstones representing mixing of source rocks after Schoenborn and Fedo (2011); (B) Granite-ultramafic end member mixing binary plot of Y/Ni vs. Cr/V after Mongelli *et al.* (2006); and (C) Ternary plot of La-Th-Sc after Jinliang and Xin (2008) representing the mixing of various source sediments for Barail sandstones.

represents a typical pattern of granitic rock (figure 8C). The provenance mixing plot of Sc vs. Th/Sc (Schoenborn and Fedo 2011) represented in figure 14(A) shows the clustering of the sandstones between high K-granite and 90% granodiorite + 10% high K-granite field.

Mongelli *et al.* (2006) proposed a binary curve mixing model between granite and ultramafic end-members by using ratios of Y/Ni vs. Cr/V which is commonly used to represent mixing of source rocks. The higher Cr/V ratio represents a mafic source, while for a granitic source the ratio is low. In figure 14(B), the Barail sandstones are representing the source more towards the granitic field (Cr/V: avg. 0.63).

Jinliang and Xin (2008) proposed a ternary plot of La-Th-Sc to represent the derivation of source sediments for sandstones due to the intermixing between granite (with Eu/Eu*: 0.5 and Th/Sc: 1.18) and granodiorite (with Eu/Eu*: 0.7 and Th/Sc: 0.5). The studied samples show possible derivation of the sediments from granitic sources with average Eu/Eu*: 0.64 and average Th/Sc: 2.66 rather than granodiorite (figure 14C).

5.3 Paleoclimatic conditions

Framework composition of sandstones and their population is controlled by the climatic conditions prevailing during the sedimentation processes. The importance of climate as a primary and early control on sand mineralogy can be demonstrated by Q-F-R (Dickinson and Suczek 1979) and $Q_p/(F+RF)$ vs. $Q_{total}/(F+RF)$ binary plot (Suttner and Dutta 1986). The bulk of ancient quartz arenite is multicyclic in origin. A unique combination of extreme conditions of climate, relief and sedimentation rate give rise to the multicyclic origin of quartz grains (Suttner and Dutta 1986). From the plot of Q-F-R, it is seen that the sands were metamorphic derived in a humid climate (figure 15A). Q-F-R contents show the high percentage of quartz in the slides (Q-F-R: 82-11-07) marking the derivation of the sands from metamorphic source. The $Q_p/(F+RF)$ vs. $Q_{total}/(F+RF)$ binary plot after Suttner and Dutta (1986) also indicates that the paleoclimatic condition was humid (figure 15B). The climatic change occurred from a semi-humid to humid climate, with the dominance of humid climate.

A semi-quantitative weathering index for sand-sized sediments which incorporates the concept of

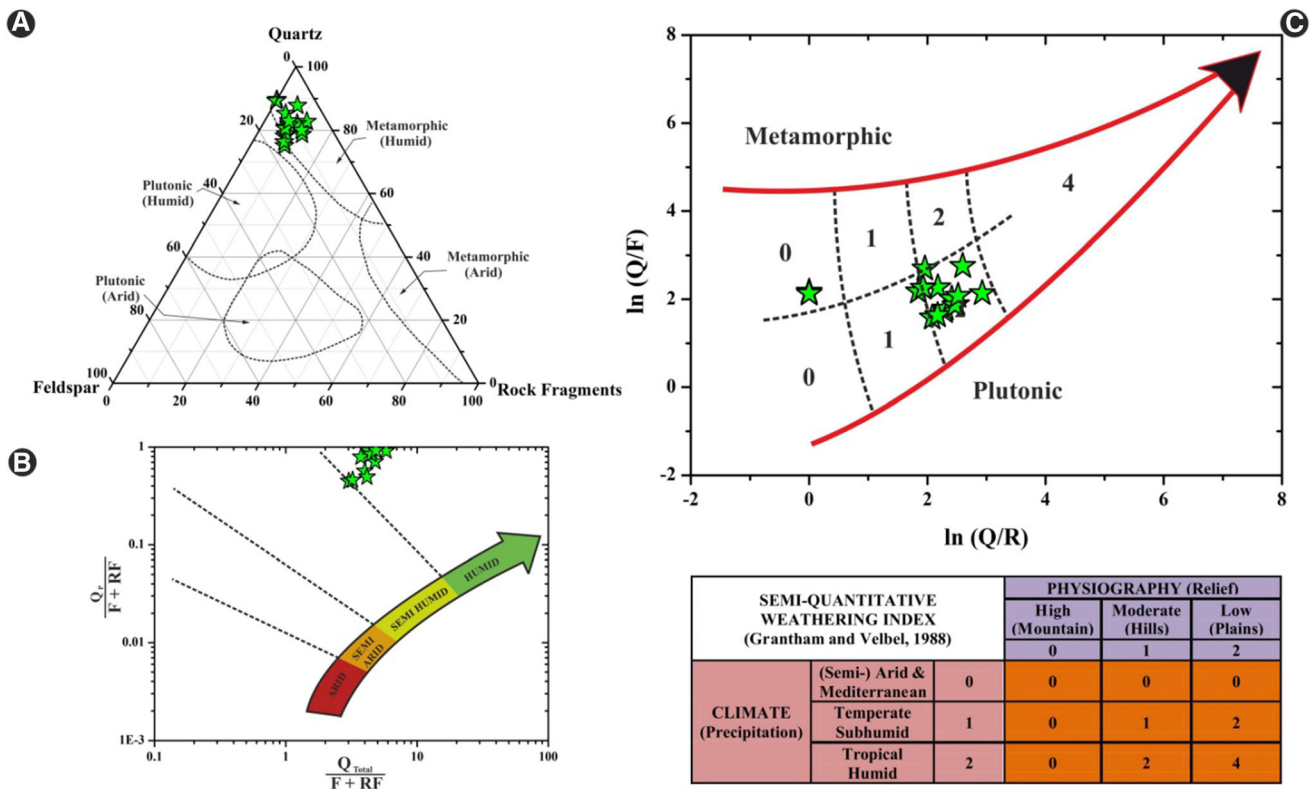


Figure 15. (A) Q–F–R ternary plot for climatic conditions after Suttner *et al.* (1981) representing humid climatic condition; (B) Bivariate plot of modal data for climatic conditions of Barail sandstones after Suttner and Dutta (1986) representing humid to semi-humid climatic conditions; and (C) Semi-quantitative weathering index after Weltje (1994) and Grantham and Velbel (1988) representing weathering indices between 1 and 2 indicating a moderate degree of weathering.

climatic and temporal threshold was proposed by Weltje (1994). It denotes the generalization of the Cumulative Chemical Weathering Index (CCWI). It was introduced by Grantham and Velbel (1988) which aimed at explaining differences in the extent of weathering from differences in effective precipitation and relief ratio between adjacent drainage basins. As per the data obtained from analyses of the sandstone samples, they were derived from lower grade metamorphics and granitic suite (figure 15C). The climate prevailing was humid with abundant rainfall (C). The relief (R) of the area was moderate (Hills), comprised mostly of low lying hills. Based on the formulae $I_w = CR$ (2) after Weltje (1994), the weathering pertaining in the area was moderate.

The petrographic results are also substantiated by various geochemical weathering indices, viz., weathering index of Parker: $[\{2(\text{Na}_2\text{O})/0.35\} + \{ \text{MgO}/0.9 \} + \{ 2(\text{K}_2\text{O})/0.25 \} + \{ \text{CaO}^*/0.7 \}] \times 100$ after Parker (1970); Chemical Index of Alteration: $[(\text{Al}_2\text{O}_3)/(\text{Al}_2\text{O}_3 + \text{CaO}^* + \text{Na}_2\text{O} + \text{K}_2\text{O})] \times 100$ after Nesbitt and Young (1982); Chemical Index of Weathering: $[(\text{Al}_2\text{O}_3)/(\text{Al}_2\text{O}_3 + \text{CaO}^* + \text{Na}_2\text{O})] \times 100$ after Harnois

(1988); Plagioclase Index of Alteration: $[(\text{Al}_2\text{O}_3 - \text{K}_2\text{O})/(\text{Al}_2\text{O}_3 + \text{CaO}^* + \text{Na}_2\text{O} - \text{K}_2\text{O})] \times 100$ after Fedo *et al.* (1995) and Index of Chemical Variability: $[(\text{Fe}_2\text{O}_3 + \text{K}_2\text{O} + \text{Na}_2\text{O} + \text{CaO}^* + \text{MgO} + \text{MnO} + \text{TiO}_2)/(\text{Al}_2\text{O}_3)]$ after Cox *et al.* (1995), etc., to decipher the paleoclimatic conditions of clastic sedimentary rocks including the extent of source rocks weathering by using major element concentrations. In the mathematical derivations of the parameters, the CaO^* indicates Ca incorporated from the silicate minerals and all the parameters are using molecular proportions of major oxides except ICV is using the weight percentage values.

Calculated average values of weathering indices of the present study are presented in table 5. An average value of Chemical Index of Alteration: 70.20 are shown by Barail sandstones which is similar to PAAS (Post-Archean Australian Shale after Taylor and McLennan 1985): 69.38. The moderate value of the CIA represents a moderate distance transportation of the sediments with less mechanical breakdown and mild chemical alteration. Also moderate CIA value along with negative Eu anomaly and low concentration of Sr

indicates some contribution of sediments from the near-most sources with higher rate of mechanical weathering exhibiting less amount of alkali-bearing minerals. We can consider that the sediments were

derived from the Himalayan ranges with some contribution from the near-most probable Indo-Burmese ranges source rocks. The representative form of CIA after Nesbitt and Young (1982) is given in figure 16(A) as a ternary plot by using the molecular proportion of $Al_2O_3-(CaO+Na_2O)-K_2O$. The samples follow a parallel trend close to the A-CN line indicating less weathering of the source rocks. Chemical Index of Weathering (CIW; Harnois 1988) is commonly used for measuring the weathering conditions. During sedimentation processes, K can be leached or gathered within the weathering products. K^+ ion associated with the pore solution can be converted to K-bearing minerals. Because of its higher ion exchange capacity, it can accommodate with the clay minerals rather than Na^+ and Ca^{2+} (Harnois 1988; Kroonenberg 1994). Similarly, the value of CIW also increases with the removal of Na and Ca with respect to Al.

Table 5. Table showing the average values of various weathering parameters.

Lithounits/standards	CIA	PIA	CIW	WIP	ICV
Barail Sandstones	70.20	77.64	81.03	38.45	1.06
UCC	50.17	50.21	55.81	69.91	1.19
GLOSS	41.16	39.57	44.56	61.72	1.59
PAAS	69.38	77.45	81.33	51.86	0.88
NASC	57.13	60.07	66.89	61.41	1.11

Note. CIA: Chemical Index of Alteration after Nesbitt and Young (1982), PIA: Plagioclase Index of Alteration after Fedo *et al.* (1995), CIW: Chemical Index of Weathering after Harnois (1988), WIP: Weathering Index of Parker after Parker (1970), ICV: Index of Chemical Variability after Cox *et al.* (1995).

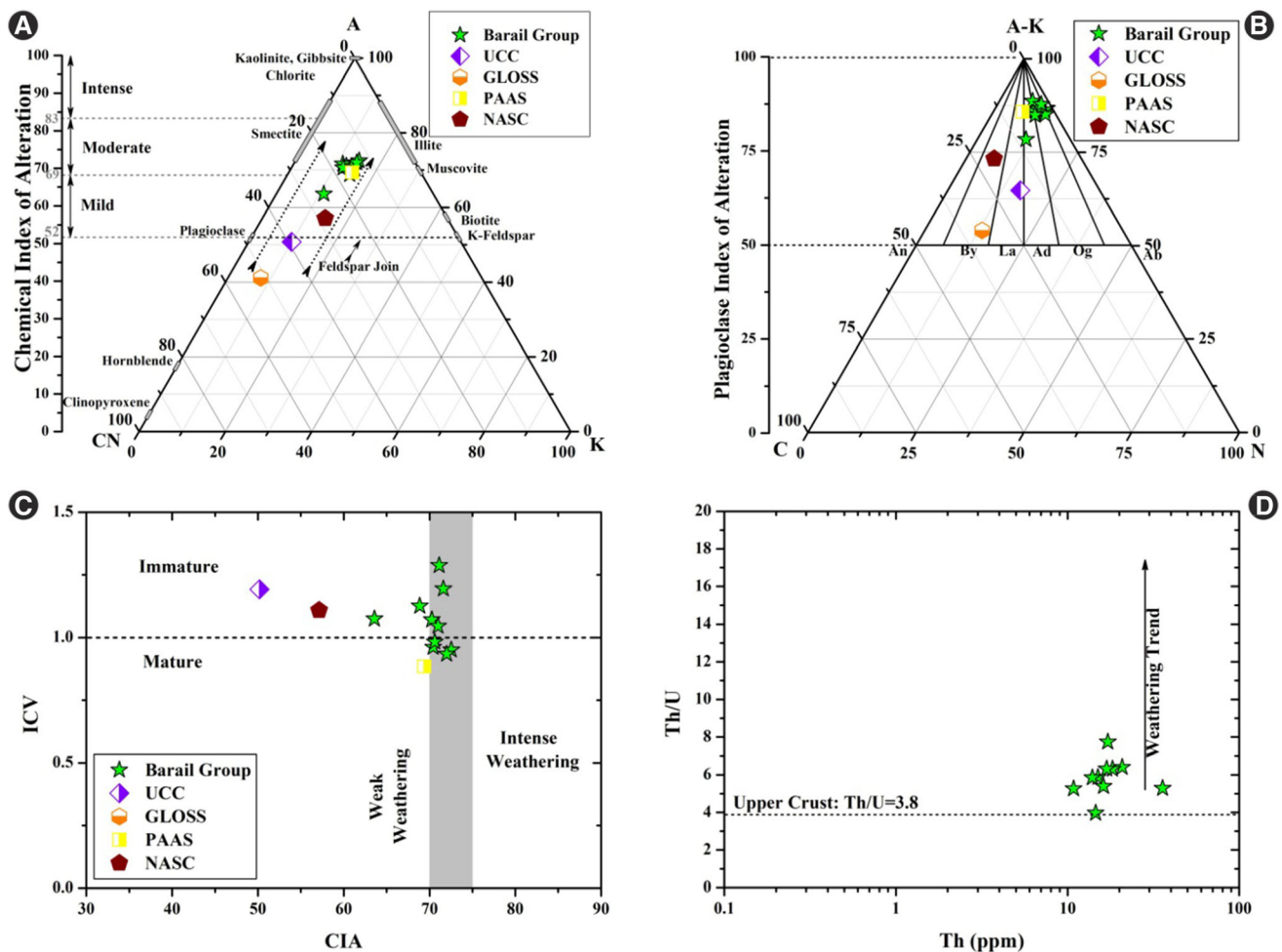


Figure 16. (A) A-CN-K plot after Nesbitt and Young (1982) representing a low to moderate nature of weathering of source rocks; (B) AK-C-N plot after Fedo *et al.* (1995) representing a moderate degree of weathering; (C) Binary plot of CIA vs. ICV after Long *et al.* (2012) representing maturity and weathering nature; and (D) Th vs. Th/U plot after McLennan and Hanson (1993) representing the weathering trend of Barail Sandstones.

The sandstones of Barail Group show moderate to higher (avg. CIW: 81.03) degree of weathering, the values of which are presented in table 5. Weathering index for plagioclase proposed by Fedo *et al.* (1995) is known as Plagioclase Index of Weathering (PIA), where wt% of alkalis are used to measure the extent of source rock weathering. Barail sandstones are showing (figure 16B) a moderate average value of PIA (77.63) which resemble with PAAS (77.45). So, it can be inferred that the source area have supplied moderately weathered to almost fresh detritus of feldspars.

Parker (1970) proposed the first chemical weathering index by using alkali and alkaline elements to measure the leached products during the sedimentation processes rather than the Si. During the hydrolysis process, most of the alkali and alkaline elements are removed. Si tends to be mobile during weathering, but the movement within a profile is irregular, and the leached or removed amount is significantly less. Therefore, Parker (1970) proposed the mobile elements like Na, Mg, K and Ca and made the base to represent the weathering index. The Barail sandstones show lower WIP value (38.45) indicating less weathered source rocks. Index of Chemical Variability (ICV; Cox *et al.* 1995) is commonly used to differentiate between clay and non-clay minerals based on the proportion of Al_2O_3 . As suggested by Cox *et al.* (1995), the range of ICV is between 0.6 and 1.0 for feldspars, illite and muscovite, while $\text{K}_2\text{O}/\text{Al}_2\text{O}_3$ ranges between 0 and 0.3 for clay minerals and 0.3–1.0 for feldspars. The Barail sandstones are showing an average of $\text{ICV}=1.06$ and $\text{K}_2\text{O}/\text{Al}_2\text{O}_3=0.17$. Based on these parameters, it can be said that Barail sandstones are composed of less amount of K-feldspars and corresponding weathered products of feldspars. The plot of CIA *vs.* ICV proposed by Long *et al.* (2012) represents (figure 16C) the maturity and weathering nature of clastic sediments. In the plot, most of the samples have the ICV value ~ 1 and average CIA (70.20). This represents that the sediments are moderately mature and recycled in nature with little amount of weak weathered product of kaolinite, smectite, illite, etc.

Binary plot of Th *vs.* Th/U after McLennan *et al.* (1993) (figure 16D) can be used to remark on the weathering behaviour of the sediments. The Th/U ratio of upper crustal rock is observed between 3.5 and 4.0 (McLennan *et al.* 1993); and values exceeding the range suggest the weathering trend. Barail sandstone shows an average value of

Th/U=5.84, which is significantly higher values than the UCC, that essentially represents undergone weathering processes. During various sedimentary processes like weathering and diagenesis, Sr leaches comparatively more than Rb because of which, the ratio of Rb/Sr increases that implies intense rate of weathering. Barail sandstones are showing an average value of Rb/Sr=1.38, representing a moderate nature of weathering. Therefore, based on the various weathering indices (avg. $I_w=2$, CIA: 70.20, CIW: 81.03, PIA: 77.63, WIP: 38.45, etc.) and certain elemental ratios (avg. Th/U: 5.84, Rb/Sr: 1.38, etc.), it is suggested that the source rock was low to moderately weathered with the dominance of humid climatic condition. Similar observations have also been reported by Hussain and Bharali (2019), based on the weathering indices of Barail sandstones of MFB (avg. CIA: 69, CIW: 77) suggested a low-moderate degree of weathering.

6. Conclusions

Based on the petrography and whole rocks geochemical analyses of the Barail sandstones studied from the MFB of Surma basin, the following conclusions are derived:

1. The Barail sandstones are mainly arkosic wacke and are less commonly sub-lithic arenite type.
2. Sediments were primarily sourced from the acidic rocks of both Himalayan and Indo-Burmese ranges with significant contribution of recycling sediments derived from near-most orogens.
3. The depositional setup for the sediments are considered to be under oceanic island arc to an active continental margin setup.
4. Sediments derived from the source areas have undergone a mild to moderate degree of weathering before the deposition took place in the basin.
5. Petrographical and geochemical data prevalence of a wet and humid paleoclimatic condition at the source area.

Acknowledgements

This research work is supported by the Department of Science and Technology-Science and Engineering Research Board (DST-SERB) vide

Letter No. EMR/2016/003915. We are grateful to the Director, National Geophysical Research Institute, Hyderabad for providing us the facilities to carry out HR-ICP-MS and XRF analysis at their laboratory. We like to thank two anonymous reviewers for their critical reviews and suggestions and Prof. Santanu Banerjee for the Editorial handling and constructive suggestions which has enhanced the quality of the manuscript.

References

- Ahmad T, Tanaka T, Sachan H K, Asahara Y, Islam R and Khanna P P 2008 Geochemical and isotopic constraints on the age and origin of the Nidar Ophiolitic Complex, Ladakh, India: Implications for the Neo-Tethyan subduction along the Indus suture zone; *Tectonophysics*. **451**(1–4) 206–224.
- Armstrong-Altrin J S 2009 Provenance of sands from Cazonas, Acapulco, and Bahía Kino beaches, México; *Revista Mexicana de Ciencias Geológicas* **26** 764–782.
- Basu A, Young S W, Suttner L J, James W C and Mack G H 1975 Re-evaluation of the use of undulatory extinction and polycrystallinity in detrital quartz for provenance interpretation; *J. Sedim. Res.* **45** 873–882, <https://doi.org/10.1306/212F6E6F-2B24-11D7-8648000102C1865D>.
- Bhaduri A 2011 State Geological and Mineral Maps – Geological Survey of India Miscellaneous Publication Series, www.indiawaterportal.org/articles/state-geology-and-mineral-maps-geological-survey-india-miscellaneous-publication-series.
- Bhatia M R 1983 Plate tectonics and geochemical composition of sandstones; *J. Geol.* **91** 611–627, <https://doi.org/10.1086/628922>.
- Bhatia M R and Crook K A W 1986 Trace element characteristics of greywackes and tectonic setting discrimination of sedimentary basins; *Contrib. Mineral. Petrol.* **92** 181–193, <https://doi.org/10.1007/BF00375292>.
- Blatt H, Middleton G and Murray R 1980 *Origin of sedimentary rocks*; Prentice-Hall, New Jersey.
- Bracciali L, Marroni M, Luca P and Sergio R 2007 Geochemistry and petrography of Western Tethys Cretaceous sedimentary covers (Corsica and Northern Apennines): From source areas to configuration of margins; *Geol. Soc. Am. Spec. Papers* **420** 73–93, [https://doi.org/10.1130/2006.2420\(06\)](https://doi.org/10.1130/2006.2420(06)).
- Chaudhuri A, Banerjee S and Chauhan G 2020 Compositional evolution of siliciclastic sediments recording the tectonic stability of a pericratonic rift: Mesozoic Kutch Basin, western India; *Mar. Petrol. Geol.* **111** 476–495, <http://doi.org/10.1016/j.marpetgeo.2019-08-026>.
- Chaudhuri A, Das K, Banerjee S and Fitzsimons I C W 2019 Detrital zircon and monazite track the source of Mesozoic sediments in Kutch to rocks of Late Neoproterozoic and Early Palaeozoic orogenies in northern India; *Gondwana Res.* **80** 188–201, <https://doi.org/10.1016/j.gr.2019.10.015>.
- Chaudhuri A, Banerjee S and Le Pera E 2018 Petrography of Middle Jurassic to Early Cretaceous sandstones in the Kutch Basin, western India: Implications on provenance and basin evolution; *J. Palaeogeogr.* **7:2**, <https://doi.org/10.1186/s42501-018-0002-6>.
- Cox R, Lowe D R and Cullers R L 1995 The influence of sediment recycling and basement composition on evolution of mudrock chemistry in the southwestern United States; *Geochim. Cosmochim. Acta* **59** 2919–2940, [https://doi.org/10.1016/0016-7037\(95\)00185-9](https://doi.org/10.1016/0016-7037(95)00185-9).
- Cullers R L 1994 The controls on the major and trace element variation of shales, siltstones, and sandstones of Pennsylvanian–Permian age from uplifted continental blocks in Colorado to platform sediment in Kansas, USA; *Geochim. Cosmochim. Acta* **58** 4955–4972, [https://doi.org/10.1016/0016-7037\(94\)90224-0](https://doi.org/10.1016/0016-7037(94)90224-0).
- Cullers R L 2000 The geochemistry of shales, siltstones and sandstones of Pennsylvanian–Permian age, Colorado, USA: Implications for provenance and metamorphic studies; *Lithos* **51** 181–200, [https://doi.org/10.1016/S0024-4937\(99\)00063-8](https://doi.org/10.1016/S0024-4937(99)00063-8).
- Cullers R L and Podkovyrov V N 2002 The source and origin of terrigenous sedimentary rocks in the mesoproterozoic Uj group, southeastern Russia; *Precamb. Res.* **117** 157–183, [https://doi.org/10.1016/S0301-9268\(02\)00079-7](https://doi.org/10.1016/S0301-9268(02)00079-7).
- Dasgupta S 1984 Tectonic trends in Surma Basin and possible genesis of the folded belt; *Rec. GSI* **113** 58–61.
- Dickinson W R 1983 Provenance of North American Phanerozoic sandstones in relation to tectonic settings; *Geol. Soc. Am. Bull.* **94** 222–235, [https://doi.org/10.1130/0016-7606\(1983\)94%3c222:PONAPS%3e2.0.CO;2](https://doi.org/10.1130/0016-7606(1983)94%3c222:PONAPS%3e2.0.CO;2).
- Dickinson W R 1985 Interpreting provenance relations from detrital modes of sandstones; In: *Provenance of Arenites, NATO ASI Series (Series C: Mathematical and Physical Sciences)*, Springer, Dordrecht 333–361, https://doi.org/10.1007/978-94-017-2809-6_15.
- Dickinson W R and Suczek C A 1979 Plate tectonics and sandstone compositions; *AAPG Bull.* **63** 2164–2182, <https://doi.org/10.1306/2F9188FB-16CE-11D7-8645000102C1865D>.
- Fedo C M, Nesbitt H W and Young G M 1995 Unravelling the effects of potassium metasomatism in sedimentary rocks and paleosols, with implications for paleoweathering conditions and provenance; *Geology* **23** 921–924, [https://doi.org/10.1130/0091-7613\(1995\)023%3c0921:UTEOPM%3e2.3.CO](https://doi.org/10.1130/0091-7613(1995)023%3c0921:UTEOPM%3e2.3.CO).
- Floyd P A and Leveridge B E 1987 Tectonic environment of the Devonian Gramscatho basin, south Cornwall: Framework mode and geochemical evidence from turbiditic sandstones; *J. Geol. Soc.* **144** 531–542, <https://doi.org/10.1144/gsjgs.144.4.0531>.
- Folk R L 1980 *Petrologie of sedimentary rocks*; <https://doi.org/10.1017/CBO9781107415324.004>.
- Franklin W A 1948 Photogeological Map, Assam & Tripura; Assam Oil Corporation Letter (Unpublished).
- Fyffe L R and Pickerill R K 1993 Geochemistry of Upper Cambrian–Lower Ordovician black shale along a north-eastern Appalachian transect; *Geol. Soc. Am. Bull.* **105** 897–910, [https://doi.org/10.1130/0016-7606\(1993\)105%3c0897:GOUCLO%3e2.3.CO;2](https://doi.org/10.1130/0016-7606(1993)105%3c0897:GOUCLO%3e2.3.CO;2).
- Ganju J L 1975 *Geology of Mizoram*; Geol. Mineralogy Metall. Soc. India, pp. 17–26.
- Gardiner N J, Hawkesworth C J, Robb L J, Whitehouse M J, Roberts N M, Kirkland C L and Evans N J 2017 Contrasting granite metallogeny through the zircon record: A case study from Myanmar; *Scientific Reports* **7:1**.

- Gazzi P 1966 Le arenarie del flysch sopracretaceo dell' Appenninomodenese; correlazioni con il flysch di Monghidoro; *Mineral. Petrogr. Acta* **12** 69–97.
- Grantham J H and Velbel M A 1988 The influence of climate and topography on rock-fragment abundance in modern fluvial sands of the southern Blue Ridge Mountains, North Carolina; *J. Sedim. Petrol.* **58** 219–227, <https://doi.org/10.1306/212F8D5F-2B24-11D7-8648000102C1865D>.
- Gromet L P, Haskin L A, Korotev R L and Dymek R F 1984 The 'North American shale composite': Its compilation, major and trace element characteristics; *Geochim. Cosmochim. Acta* **48(12)** 2469–2482.
- Gu X X, Liu J M, Zheng M H, Tang J X and Qi L 2002 Provenance and tectonic setting of the proterozoic turbidites in Hunan, South China: Geochemical evidence; *J. Sedim. Res.* **72** 393–407, <https://doi.org/10.1306/081601720393>.
- Harnois L 1988 The CIW index: A new chemical index of weathering; *Sedim. Geol.* **55** 319–322, [https://doi.org/10.1016/0037-0738\(88\)90137-6](https://doi.org/10.1016/0037-0738(88)90137-6).
- Hayashi K I, Fujisawa H, Holland H D and Ohmoto H 1997 Geochemistry of ~1.9 Ga sedimentary rocks from northeastern Labrador, Canada; *Geochim. Cosmochim. Acta* **61** 4115–4137, [https://doi.org/10.1016/S0016-7037\(97\)00214-7](https://doi.org/10.1016/S0016-7037(97)00214-7).
- Hayman R J 1937 Reconnaissance map of part of Lushai Hills; *Report R. J. H.* **11** (Unpublished Burma Oil Company Report).
- Herron M M 1988 Geochemical classification of terrigenous sands and shales from core or log data; *SEPM J. Sedim. Res.* **58**, <https://doi.org/10.1306/212F8E77-2B24-11D7-8648000102C1865D>.
- Hossain H M Z, Roser B P and Kimura J I 2010 Petrography and whole-rock geochemistry of the Tertiary Sylhet succession, northeastern Bengal Basin, Bangladesh: Provenance and source area weathering; *Sedim. Geol.* **228** 171–183, <https://doi.org/10.1016/j.sedgeo.2010.04.009>.
- Hussain M F and Bharali B 2019 Whole-rock geochemistry of Tertiary sediments of Mizoram Foreland Basin, NE India: Implications for source composition, tectonic setting and sedimentary processes; *Acta Geochemica*, <https://doi.org/10.1007/s11631-019-00315-3>.
- Jiang Z, Wang Q, Wyman D A, Shi X, Yang J, Ma L and Gou G 2015 Zircon U–Pb geochronology and geochemistry of Late Cretaceous–early Eocene granodiorites in the southern Gangdese batholith of Tibet: Petrogenesis and implications for geodynamics and Cu Au Mo mineralization; *Int. Geol. Rev.* **57(3)** 373–392.
- Jinliang Z and Xin Z 2008 Composition and Provenance of sandstones and siltstones in Paleogene, Huimin Depression, Bohai Bay Basin, eastern China; *J. China Univ. Geosci.* **19** 252–270, [https://doi.org/10.1016/S1002-0705\(08\)60044-8](https://doi.org/10.1016/S1002-0705(08)60044-8).
- Kroonenberg S B 1994 Effects of provenance, sorting and weathering on the geochemistry of fluvial sands from different tectonic and climatic environments; *Proc. 29th Int. Geol. Congress*, **Part A** 69–81.
- La Touche T H D 1891 Note on the geology of Lushai Hills; *Rec. Geol. Surv. India* **24** 83–141.
- Long X, Yuan C, Sun M, Safonova I, Xiao W and Wang Y 2012 Geochemistry and U–Pb detrital zircon dating of Paleozoic graywackes in East Junggar, NW China: Insights into subduction–accretion processes in the southern Central Asian Orogenic Belt; *Gondwana Res.* **21** 637–653, <https://doi.org/10.1016/j.gr.2011.05.015>.
- McLennan S M, Hemming S, McDaniel D K and Hanson G N 1993 Geochemical approaches to sedimentation, provenance, and tectonics; *Geol. Soc. Am. Spec. Paper* **284** 21–40.
- Mongelli G, Critelli S, Perri F, Sonnino M and Perrone V 2006 Sedimentary recycling, provenance and paleoweathering from chemistry and mineralogy of Mesozoic continental red bed mudrocks, Peloritani mountains, southern Italy; *Geochem. J.* **40** 197–209, <https://doi.org/10.2343/geochemj.40.197>.
- Najman Y and Garzanti E 2000 Reconstructing early Himalayan tectonic evolution and paleogeography from Tertiary foreland basin sedimentary rocks, northern India; *GSA Bull.* **112(3)** 435–449, [https://doi.org/10.1130/0016-7606\(2000\)112<435:REHTEA>2.0.CO;2](https://doi.org/10.1130/0016-7606(2000)112<435:REHTEA>2.0.CO;2).
- Nandy D R, Dasgupta S, Sarkar K and Ganguly A 1983 Tectonic evolution of Tripura–Mizoram Fold Belt, Surma Basin, northeast India; *Quart. J. Geol. Min. Met. Soc. India* **55** 186–194.
- Nesbitt H W and Young G M 1982 Early proterozoic climates and plate motions inferred from major element chemistry of lutites; *Nature* **299** 715–717, <https://doi.org/10.1038/299715a0>.
- Paikaray S, Banerjee S and Mukherji S 2008 Geochemistry of shales from the Paleoproterozoic to Neoproterozoic Vindhyan Supergroup: Implications on provenance, tectonics and paleoweathering; *J. Asian Earth Sci.* **32** 34–48, <https://doi.org/10.1016/j.jseae.2007.10.002>.
- Parker A 1970 An index of weathering for silicate rocks; *Geol. Mag.* **107** 501–504, <https://doi.org/10.1017/S0016756800058581>.
- Pettijohn F J, Potter P E and Siever R 1972 *Sand and sandstones*; New York, Springer-Verlag.
- Ram J and Venkataraman B 1984 Tectonic framework and hydrocarbon prospects of Mizoram; In: *Petroliferous Basins of India, Petrol. Asia J.* **2** 60–65.
- Reichardt H, Weinberg R F, Andersson U B and Fanning C M 2010 Hybridization of granitic magmas in the source: The origin of the Karakoram Batholith, Ladakh, NW India; *Lithos* **116(3–4)** 249–272.
- Rudnick R L and Gao S 2003 Composition of the continental crust; *The Crust* **3** 1–64.
- Saha S, Banerjee S, Burley S D, Ghosh A and Saraswati P K 2010 The influence of flood basaltic source terrains on the efficiency of tectonic setting discrimination diagrams: An example from the Gulf of Khambhat, western India; *Sedim. Geol.* **228** 1–13, <https://dx.doi.org/10.1016/j.sedgeo.2010.03.009>.
- Saha S, Burley S D and Banerjee S 2017 Mixing processes in modern estuarine sediments from the Gulf of Khambhat, western India; *Mar. Petrol. Geol.* **91** 599–621, <https://doi.org/10.1016/j.marpetgeo.2017.12.010>.
- Sawant S S, Kumar K V, Balaram V, Subba Rao D V, Rao K S and Tiwari R P 2017 Geochemistry and genesis of Craton-derived sediments from active continental margins: Insights from the Mizoram Foreland Basin, NE India; *Chem. Geol.* **470** 13–32.
- Schoenborn W A and Fedo C M 2011 Provenance and paleoweathering reconstruction of the Neoproterozoic Johnnie Formation, southeastern California; *Chem. Geol.* **285** 231–255, <https://doi.org/10.1016/j.chemgeo.2011.04.014>.
- Suttner L, Basu A and Mack G H 1981 Climate and the origin of quartz arenites; *J. Sedim. Petrol.* **51** 1235–1246.

- Suttner L J and Dutta P K 1986 Alluvial sandstone composition and paleoclimate, I. Framework mineralogy; *J. Sedim. Petrol.* **56** 329–345, <https://doi.org/10.1306/212F8909-2B24-11D7-8648000102C1865D>.
- Taylor S R and McLennan S M 1985 The continental crust: Its composition and evolution; Oxford University, Blackwell, London.
- Tiwari R P and Kachhara R P 2003 Molluscan biostratigraphy of the tertiary sediments of Mizoram, India; *J. Paleontol. Soc. India, Lucknow* **48** 59–82.
- Tiwari R P, Malsawma J, Sangode S J and Arora B R 2007 Magnetostratigraphy of a part of Middle Bhuban sequence (Surma Group), Aizawl, Mizoram; *J. Geol. Soc. India* **70** 667–674.
- Tiwari R P, Rajkonwar C, Lalchawimawii, Malsawma J, Ralte V Z and Patel S J 2011 Trace fossils from Bhuban formation, Surma group (Lower to Middle Miocene) of Mizoram India and their Palaeoenvironmental significance; *J. Earth Syst. Sci.* **120** 1127–1143, <https://doi.org/10.1007/s12040-011-0131-0>.
- Tortosa A, Palomares M and Arribas J 1991 Quartz grain types in Holocene deposits from the Spanish Central System: Some problems in provenance analysis; *Geol. Soc. London, Spec. Publ.* **57** 47–54, <https://doi.org/10.1144/GSL.SP.1991.057.01.05>.
- Uddin A and Lundberg N 1998 Cenozoic history of the Himalayan-Bengal system: Sand composition in the Bengal basin, Bangladesh; *Bull. Geol. Soc. Amer.* **110**(4) 497–511.
- Weltje G J 1994 Provenance and dispersal of sand-sized sediments: Reconstruction of dispersal patterns and sources of sand-sized sediments by means of inverse modelling techniques; *Geologica Ultraiectina*, <http://dspace.library.uu.nl/handle/1874/274730>.
- Xu Y, Liu C Z, Chen Y, Guo S, Wang J G and Sein K 2017 Petrogenesis and tectonic implications of gabbro and plagiogranite intrusions in mantle peridotites of the Myitkyina ophiolite, Myanmar; *Lithos* **648** (284–285) 180–193.
- Zeng L, Gao L E, Tang S, Hou K, Guo C and Hu G 2014 Eocene magmatism in the Tethyan Himalaya, southern Tibet; *Geol. Soc. London, Spec. Publ.* **SP412**.

Corresponding editor: SANTANU BANERJEE